N-Body Oscillator Interactions of Higher-Order Coupling Functions*

Youngmin Park[†] and Dan Wilson[‡]

Abstract. We introduce a method to identify phase equations that include N-body interactions for general coupled oscillators valid far beyond the weak coupling approximation. This strategy is an extension of the theory from [Y. Park and D. Wilson, SIAM J. Appl. Dyn. Syst., 20 (2021), pp. 1464–1484] and yields coupling functions for $N \geq 2$ oscillators for arbitrary types of coupling (e.g., diffusive, gap-junction, chemical synaptic). These coupling functions enable the study of oscillator networks in terms of phase-locked states, whose stability can be determined using straightforward linear stability arguments. We demonstrate the utility of our approach with two examples. First, we use a diffusely coupled complex Ginzburg–Landau (CGL) model with N=3 and show that the loss of stability in its splay state occurs through a Hopf bifurcation viewing the nonweak diffusive coupling as the bifurcation parameter. Our reduction also captures asymptotic limit-cycle dynamics in the phase differences. Second, we use N=3 realistic conductance-based thalamic neuron models and show that our method correctly predicts a loss in stability of a splay state for nonweak synaptic coupling. In both examples, our theory accurately captures model behaviors that weak and recent nonweak coupling theories cannot.

Key words. phase reduction, coupled oscillators, coupling functions, oscillators

MSC codes. 92B25, 92E99, 92F99

DOI. 10.1137/23M1594182

1. Introduction. Oscillatory phenomena exist in many biological [3, 72, 60, 24, 73], chemical [27, 13], and physical systems [44]. Numerical models that capture the important behaviors of these systems often involve complex interactions of large numbers of variables, reducing the visibility of important mechanisms. As such, phase reduction is often used for understanding the aggregate behavior of interacting oscillators in a reduced-order setting [27, 24, 17, 48, 16].

The many techniques developed for phase reduction often include specific assumptions that improve tractability at the cost of biological relevance. The Kuramoto model is an exceptionally well-studied model, owing to its elegant simplicity, and has proven invaluable towards understanding higher-order interactions and stable synchronous network states [29]. However, the Kuramoto model was originally derived in the case of infinite, homogeneous, globally coupled oscillators [12] near the Hopf bifurcation [30], limiting its use for finite populations away from the Hopf. Moreover, its analysis is often limited to studying questions

^{*}Received by the editors August 15, 2023; accepted for publication (in revised form) by J. Rubin April 9, 2024; published electronically June 13, 2024.

https://doi.org/10.1137/23M1594182

Funding: The work of the second author was supported by National Science Foundation grant NSF-2140527.

[†]Department of Mathematics, University of Florida, Gainesville, FL 32601 USA (ympark1988@gmail.com, https://youngmp.github.io).

[‡]Department of Electrical Engineering and Computer Science, University of Tennessee, Knoxville, TN 37996 USA (dwilso81@utk.edu, https://volweb.utk.edu/~dwilso81).

around synchrony as opposed to other phase-locking phenomena, due to the often-taken limit of infinite oscillators.

When a finite number of oscillators is considered, other features may be exploited, each with their own limitations. When the network exhibits symmetries, it is possible to enumerate all phase-locked states with weak or strong coupling [20], but this method is not suited to work in the case of asymmetries [23]. In networks of neurons, the pulse-like shape of action potentials allows for the use of pulse coupling [11, 5, 4, 52, 40]. This approach yields analytically tractable results for weak or strong and possibly asymmetric coupling, but the number of oscillators is often limited to pairs. The study of network behavior can be made tractable by using piecewise smooth models, but coupling functions require particular assumptions such as linear coupling [9, 8], weak coupling [7, 49], and Laplacian coupling [43]. In addition, the analysis of phase-locked states is often restricted to understanding the stability of a synchronous network state [8, 10] (although some do consider the stability of splay states [7]).

The most relevant reduction for the present study is the theory of weakly coupled oscillators, which allows for a general form of the vector field and coupling function so long as the coupling strength is weak [15, 26, 46, 48, 49, 47]. To be more precise, by weak coupling, we mean phase reductions that only consider expansions up to first order in coupling strength (often represented by ε), and are thus generally only guaranteed to be valid for arbitrarily small ε . The weak assumption is a severe limitation because it cannot necessarily be used to accurately capture the dynamical behavior of coupled oscillator networks in many biological networks, e.g., cortical networks [53, 6], subcortical networks [62], and pacemaker networks [3, 19]. Indeed, recent studies have pushed beyond the weak coupling regime by deriving correction terms in higher orders of the coupling strength (i.e., nonweak coupling), but these too have their limitations. Higher-order phase correction terms considered in [55, 18, 64] require the underlying limit cycle to be strongly attracting, limiting their applicability when Floquet multipliers are close to unity [67]. Recently developed isostable coordinates have proven invaluable towards developing more robust phase reductions, e.g., [69, 50, 42]. However, these methods have only been applied to pairs of oscillators without heterogeneity (except in [42], where the authors consider the complex Ginzburg-Landau model for $N \geq 2$ and the Morris-Lecar model for N=200), and a recently published article by [34] closely mirrors our assumptions, but is only valid for planar systems. The recent work by Nicks, Allen, and Coombes [42] is of significant relevance to this paper, and we briefly contrast our results in the discussion in section 6.

In networks consisting of more than two oscillators, N-body interactions on simplicial complexes become relevant. Much recent work has been done to develop phase reductions in this direction, but the study of N-body interactions have been limited to tractable models such as the Kuramoto model [59, 61, 58, 2] or the Ginzburg-Landau equation [29]. Finally, note that these studies begin with higher-order interactions as an assumption, in contrast to [69], where it is shown that higher-order interactions emerge as a function of higher-order corrections to weak coupling theory. Thus, there exists no phase-isostable reduction method for general n-dimensional oscillators that accounts for heterogeneity, strong coupling, and resulting N-body interactions.

In the present study, we address this gap in the literature by deriving a phase reduction method applicable to networks of (weakly or strongly attracting) coupled oscillators with

arbitrary network topology beyond weak coupling, i.e., we calculate higher-order corrections to the first-order reduction methods while incorporating isostable coordinate(s). The formulation includes N-body interactions on simplicial complexes and enables us to study the existence and stability of phase-locked states in a manner not possible using the original models.

The paper is organized as follows. We derive the proposed phase-isostable reduction in section 3 and check the performance of our method using the complex Ginzburg–Landau (CGL) model (with some analytical calculations) in section 4. We also confirm that our method works using the neurobiologically realistic thalamic model in section 5. Stability of splay states as a function of coupling strength are discussed as part of these results. We conclude the paper with a discussion in section 6.

All code used to generate figures is available for public use at https://github.com/youngmp/nbody [45].

2. Background.

2.1. Phase and phase reduction. Consider a general dynamical system

$$\dot{X} = F(X) + U(X, t),$$

where $X \in \mathbb{R}^n$ is the state, $F : \mathbb{R}^n \to \mathbb{R}^n$ is a smooth vector field, and $U(X,t) \in \mathbb{R}^n$ is some additive input. Let Y be a stable T-periodic orbit that emerges when taking U(X,t) = 0. In situations where the timing of oscillations is of interest, it can be useful to consider the dynamics of (2.1) in terms of a scalar phase $\theta(X) \in \mathbb{S}^1$ rather than in terms of the state. When U(X,t) = 0, the notion of isochrons [21] can be used to define phase in the basin of attraction of the limit cycle. Isochrons can be defined as follows: letting $\theta_1 \in [0,1)$ be the phase associated with an initial condition $a(0) \in Y$, the θ_1 isochron is composed of the set of all b(0) for which

(2.2)
$$\lim_{t \to \infty} ||a(t) - b(t)|| = 0,$$

where $||\cdot||$ can be any vector norm. Isochrons are typically scaled so that $\frac{d\theta}{dt}$ is a constant for trajectories that evolve under the unperturbed flow of the vector field; in this work, we choose $\frac{d\theta}{dt} = 1$ for convenience.

Working in phase coordinates, by restricting one's attention to a close neighborhood of the periodic orbit and allowing $U(X,t) \neq 0$, through a change of coordinates one arrives at the standard phase reduction [17, 24, 27]

$$\frac{d\theta}{dt} = \frac{\partial \theta}{\partial X} \cdot \frac{dX}{dt}$$

$$= \frac{\partial \theta}{\partial X} \cdot (F(X) + U(X, t))$$

$$= 1 + \mathcal{Z}(\theta) \cdot U(X, t),$$
(2.3)

where $\mathcal{Z}(\theta) = \frac{\partial \theta}{\partial X}$ evaluated on the periodic orbit at phase θ , and the "dot" denotes the dot product. In the third line above, we use the fact that $\frac{\partial \theta}{\partial X} \cdot F(X)$ was scaled to equal 1. Reductions of the form (2.3) have been used widely as a starting point for the analysis of weakly perturbed and weakly coupled oscillatory systems [17, 54, 41, 71].

2.2. Isostable coordinates. In (2.3), the gradient of the phase is evaluated on the periodic orbit. As such, it requires the state X to remain close to Y for the reduction to remain valid. This is only guaranteed in the limit of weak forcing; in many practical applications, alternative techniques that can accommodate stronger forcing must be used. One common strategy is to augment the phase coordinates with amplitude coordinates. A variety of techniques for considering both phase and amplitude coordinates have been proposed [70, 55, 65, 68, 57].

In this work, we use the phase-isostable coordinate system, which augments the phase dynamics with additional information about level sets of the slowest decaying modes of the Koopman operator [35, 38]. To illustrate this coordinate system, let U(X,t) = 0 and define $\Delta X = X - Y(\theta)$. To a linear approximation the dynamics of (2.1) follow

$$\Delta \dot{X} = J \Delta X,$$

where J is the Jacobian evaluated at $Y(\theta(t))$. Notice that (2.4) is linear and time-varying with the Jacobian being T-periodic. Let Φ be the fundamental matrix, i.e., with $\Delta X(T) = \Phi \Delta X(0)$ for initial conditions $\theta(X(0)) \approx 0$. Further, let w_j, v_j , and λ_j be left eigenvectors, right eigenvectors, and associated eigenvalues, respectively, of Φ . Floquet exponents can be computed according to $\kappa_j = \log(\lambda_j)/T$. Let κ_1 be the slowest decaying nonzero Floquet exponent. If κ_1 is unique, an associated isostable coordinate can be defined in the basin of attraction of the limit cycle according to [67]

(2.5)
$$\psi_1(X) = \lim_{k \to \infty} (w_1^\top (\eta(t_\Gamma^k, X) - Y_0) \exp(-\kappa_1 t_\Gamma^k)),$$

where t_{Γ}^k denotes the time of the kth transversal of the $\theta=0$ isochron, $\eta(t,X)$ is the unperturbed flow of the vector field that takes X(0) to X(t), Y_0 is the intersection of the periodic orbit and the $\theta=0$ isochron, and $^{\top}$ denotes the transpose. In contrast to isochrons defined in (2.2), which characterize the infinite time convergence to the periodic orbit, the isostable coordinates defined in (2.5) give a sense of the distance from the periodic orbit, with larger $|\psi_1(X)|$ values corresponding to states that will take longer to approach the periodic orbit. Isostable coordinates can also be used to characterize faster decaying components of the solution, but an explicit definition akin to (2.5) is not always possible [28]. Instead, faster decaying isostable coordinates can be defined as level sets of appropriately chosen Koopman eigenfunctions. In this work, we will assume that the faster decaying isostable coordinates decay rapidly and are well approximated by zero. Using (2.5), it is possible to show directly that when U(X,t)=0, $\frac{d\psi_1}{dt}=\kappa_1\psi_1$ in the basin of attraction of the limit cycle [67].

2.3. Phase-isostable reduction. Information about the slowest decaying isostable coordinate can be used to augment standard phase models of the form (2.3) to increase the accuracy of the reduction in response to larger magnitude inputs. In the analysis in the following sections, we assume that all nonzero Floquet exponents except κ_1 have a large real component so that the associated isostable coordinates decay rapidly and are well approximated by zero. Moving forward, for notational convenience, we will simply use ψ and κ to denote the only nontruncated isostable coordinate and its Floquet exponent—from this point forward, subscripts of any variable including ψ and κ will only denote the oscillator index. Taking this isostable coordinate into account, one can consider a modified version of (2.3),

(2.6)
$$\dot{\theta} = 1 + \mathcal{Z}(\theta, \psi) \cdot U(X, t),$$

where the gradient of the phase is not necessarily evaluated on the periodic orbit, but rather at a state corresponding to $X(\theta, \psi)$; note that $X(\theta, 0) = Y(\theta)$. In order to use (2.6), it is necessary to consider the isostable coordinate dynamics as well as the phase dynamics. Considering the dynamics given by (2.1), by the chain rule,

$$\frac{d\psi}{dt} = \frac{\partial \psi}{\partial X} \cdot \frac{dX}{dt}
= \frac{\partial \psi}{\partial X} \cdot (F(X) + U(X, t))
= \kappa \psi + \mathcal{I}(\theta, \psi) \cdot U(X, t),$$
(2.7)

where $\mathcal{I}(\theta,\psi) = \frac{\partial \psi}{\partial X}$ evaluated at $X(\theta,\psi)$. In the third line above, the relationship $\frac{\partial \psi}{\partial X} \cdot F(x) = \kappa \psi$ since $\frac{d\psi}{dt} = \kappa \psi$ when U(X,t) = 0. Taken together, (2.6) and (2.7) comprise the phase-isostable reduction. For computation and analysis purposes, the gradient of the phase and isostable coordinate is often represented according to a Taylor expansion in the isostable coordinate centered at $\psi = 0$:

(2.8)
$$\dot{\theta} = 1 + (Z^{(0)}(\theta) + \psi Z^{(1)}(\theta) + \psi^2 Z^{(2)}(\theta) + \cdots) \cdot U(X, t),$$

$$\dot{\psi} = \kappa \psi + (I^{(0)}(\theta) + \psi I^{(1)}(\theta) + \psi^2 I^{(2)}(\theta) + \cdots) \cdot U(X, t).$$

3. Higher-order coupling with N-body interactions. We now derive a reduced system of phase equations that captures higher-order interactions between coupled oscillators, starting with the ordinary differential equation (ODE)

(3.1)
$$\dot{X}_{i} = F_{i}(X_{i}) + \delta_{i}Q_{i}(X_{i}) + \varepsilon \left[\sum_{j=1}^{N} a_{ij}G_{ij}(X_{i}, X_{j}) \right], \quad i = 1, 2, \dots, N,$$

where each system admits a T-periodic limit cycle $Y_i(t)$ when $\delta_i = \varepsilon = 0$. We assume, when $\delta_i, \varepsilon \neq 0$, that δ_i and ε are not necessarily small, and that δ_i is order $O(\varepsilon)$. Thus, while the derivation to follow is constrained by ε , heterogeneity and coupling need not be weak in the sense that we seek to capture higher-order corrections to first-order phase dynamics.

We assume general smooth vector fields $F_i: \mathbb{R}^{n_i} \to \mathbb{R}^{n_i}$, smooth coupling functions $G_{ij}: \mathbb{R}^{n_i} \times \mathbb{R}^{n_j} \to \mathbb{R}^{n_i}$, and smooth additive heterogeneity $Q_i: \mathbb{R}^{n_i} \to \mathbb{R}^{n_i}$, where $n_i \in \mathbb{N}$ for each oscillator i. The scalars a_{ij} modulate coupling strength between pairs of oscillators and determine network topology, whereas ε modulates the overall coupling strength of the network.

Remarks.

• Oscillators need not necessarily share the same period to apply the proposed method. Requiring all oscillators to have the same period when $\delta_i = \varepsilon = 0$ is a matter of convenience, but equivalent to heterogeneity in the following sense. The dynamics of node i without coupling ($\varepsilon = 0$) are given by $\dot{X}_i = F_i(X_i, c_i^*) + \delta_i Q_i(X_i)$, where c_i^* is a particular choice of a parameter in F_i such that when $\delta_i = 0$, the stable limit cycle of the node dynamics $Y_i(t, c_i^*)$ has period T for each i. While we require that $|c_i - c_i^*| = O(\varepsilon)$ for all i, we remind the reader that ε is not necessarily small—and our method is designed to capture potential higher-order effects. This property is the same as that considered in [34]—we save a more detailed comparison for the discussion in

section 6. As a natural example, it is reasonable to expect such c_i^* to exist in multiple heterogeneous neural oscillators by adjusting their individual input currents, with the caveat that the heterogeneity is not too large.

- The choice of heterogeneity in (3.1) implicitly restricts our attention to cases where the difference $c_i c_i^* = \delta_i$ yields a linear change in each vector field. However, non-linear changes may be incorporated by including additional higher-order terms in δ_i (we elaborate more on this feature at the end of the phase difference derivation in section 3.3).
- In principle, there may be any number of heterogeneous parameters per oscillator (as opposed to one c_i^* per oscillator i), but we restrict our attention to the simple case of one heterogeneous parameter across all oscillators ($\delta_i \equiv \delta$) because the primary goal of the present study is to verify that our proposed phase reduction accurately captures higher-order interactions due to *coupling*.

We assume that there is only one nontrivial isostable coordinate similar to prior studies [67, 69, 50] and let $\kappa_i < 0$ be the corresponding Floquet exponent, where we place no restrictions on the spread of κ_i between oscillators (we reiterate that the subscript i denotes the oscillator index, so κ_i is not the ith Floquet exponent of a given oscillator, but rather the Floquet exponent of the nontrivial isostable coordinate of oscillator i).

We reduce (3.1) to phase-amplitude coordinates using phase-isostable reduction of the form (2.6) and (2.7):

$$\dot{\theta}_{i} = 1 + \delta \mathcal{Z}_{i}(\theta_{i}, \psi_{i}) \cdot Q_{i}(\theta_{i}, \psi_{i}) + \varepsilon \mathcal{Z}_{i}(\theta_{i}, \psi_{i}) \cdot \sum_{j=1}^{N} a_{ij} G_{ij}(\theta_{i}, \psi_{i}, \theta_{j}, \psi_{j}),$$

$$\dot{\psi}_{i} = \kappa_{i} \psi_{i} + \delta \mathcal{I}_{i}(\theta_{i}, \psi_{i}) \cdot Q_{i}(\theta_{i}, \psi_{i}) + \varepsilon \mathcal{I}_{i}(\theta_{i}, \psi_{i}) \cdot \sum_{j=1}^{N} a_{ij} G_{ij}(\theta_{i}, \psi_{i}, \theta_{j}, \psi_{j}),$$

where θ_i represents the oscillator phase, ψ_i represents the amplitude of a trajectory perturbed away from the underlying limit cycle, \mathcal{Z}_i is the gradient of the phase often referred to as the phase response curve (PRC), and \mathcal{I}_i is the gradient of the isostable coordinate often referred to as the isostable response curve (IRC). We suppress the time dependence of θ_i and ψ_i to reduce notational clutter.

3.1. Expansions. An important step towards reducing (3.1) involves taking the Taylor expansion of all terms with respect to ψ_i and ε . Assuming that the functions \mathcal{Z}_i and \mathcal{I}_i are sufficiently smooth within their respective basins of attraction, their approximations may be obtained to high degrees of accuracy by computing the coefficients of ψ_i as in (2.7) (see [66, 51]):

(3.3)
$$\mathcal{Z}_{i}(\theta, \psi) \approx Z_{i}^{(0)}(\theta) + \psi Z_{i}^{(1)}(\theta) + \psi^{2} Z_{i}^{(2)}(\theta) + \cdots,$$

(3.4)
$$\mathcal{I}_{i}(\theta, \psi) \approx I_{i}^{(0)}(\theta) + \psi I_{i}^{(1)}(\theta) + \psi^{2} I_{i}^{(2)}(\theta) + \cdots,$$

(3.5)
$$X_i(t) \approx Y_i(\theta_i) + \psi_i g_i^{(1)}(\theta_i) + \psi_i^2 g_i^{(2)}(\theta_i) + \cdots,$$

where $Z_i^{(k)}$, $I_i^{(k)}$, and $g_i^{(k)}$ are the higher-order correction terms to the infinitesimal (linear) PRC, infinitesimal (linear) IRC, and Floquet eigenfunction, respectively. We make an additional ansatz that each isostable coordinate ψ_i can be expressed as order $O(\varepsilon)$ deviations from $\psi_i = 0$ due to coupling and heterogeneity, and that corrections to the order $O(\varepsilon)$ term can be computed directly from higher-order Taylor expansions. Thus,

(3.6)
$$\psi_i(t) \approx \varepsilon p_i^{(1)}(t) + \varepsilon^2 p_i^{(2)}(t) + \varepsilon^3 p_i^{(3)}(t) + \cdots$$

We assume that we have calculated solutions $Z_i^{(k)}$, $I_i^{(k)}$, and $g_i^{(k)}$ for each i = 1, ..., N and $k \in \mathbb{N}$, for instance, using methods described in [66].

Some care must be taken when obtaining ε -expansions for the coupling functions G_{ij} (in contrast to the ε -expansion of \mathcal{Z}_i , \mathcal{I}_i , and X_i , which is a straightforward matter of substituting (3.6) into (3.3), (3.4), and (3.5), respectively). Let us fix a particular pair of oscillators i and j. We use the Floquet eigenfunction approximation for each oscillator,

(3.7)
$$\Delta x_i \approx \psi_i g_i^{(1)}(\theta_i) + \psi_i^2 g_i^{(2)}(\theta_i) + \cdots,$$

where $\Delta x_i \equiv X_i(t) - Y_i(\theta_i(t))$ is the difference between the limit cycle Y_i and trajectory X_i . Δx_j has an identical expression in terms of j instead of i. We view the coupling function as the map $G_{ij}: \mathbb{R}^{n_i+n_j} \to \mathbb{R}^{n_i}$, where $G_{ij}(\Xi_{ij}) = [G_{ij,1}(\Xi_{ij}), G_{ij,2}(\Xi_{ij}), \dots, G_{ij,n}(\Xi_{ij})]^{\top} \in \mathbb{R}^{n_i}$, $G_{ij,m}: \mathbb{R}^{n_i+n_j} \to \mathbb{R}$, and $\Xi_{ij} = [X_i^{\top}, X_j^{\top}]^{\top} \in \mathbb{R}^{n_i+n_j}$, an $(n_i + n_j) \times 1$ column vector. Define $\Lambda_{ij} = [Y_i(\theta_i)^{\top}, Y_j(\theta_j)^{\top}]^{\top} \in \mathbb{R}^{n_i+n_j}$ and $\Delta \Xi_{ij} = [\Delta x_i^{\top}, \Delta x_j^{\top}]^{\top} \in \mathbb{R}^{n_i+n_j}$. Both are $(n_i + n_j) \times 1$ column vectors, so that the relation $\Xi_{ij} = \Lambda_{ij} + \Delta \Xi_{ij}$ is well defined.

We apply the standard definition of higher-order derivatives from [33, 66] to obtain the multivariate Taylor expansion of $G_{ij,m}$ for each m = 1, 2, ..., n:

$$(3.8) \quad G_{ij,m}(\Lambda_{ij} + \Delta \Xi_{ij}) = G_{ij,m}(\Lambda_{ij}) + G_{ij,m}^{(1)}(\Lambda_{ij}) \Delta \Xi_{ij} + \sum_{k=2}^{\infty} \frac{1}{k!} \left[\bigotimes^{k} \Delta \Xi_{ij}^{\top} \right] \operatorname{vec} \left(G_{ij,m}^{(k)}(\Lambda_{ij}) \right),$$

where the "vec" operator simply reshapes a matrix by stacking its columns, allowing us to avoid calculating high-dimensional tensors. For example, if an $m \times n$ matrix A has columns a_i for i = 1, ..., n for $a_i \in \mathbb{R}^m$, then vec(A) is the $mn \times 1$ column vector $(a_1^{\top}, a_2^{\top}, ..., a_n^{\top})^{\top}$. If A is a Jacobian matrix, taking partial derivatives of vec(A) yields a matrix, whereas taking partial derivatives of A yields a tensor. Both contain the same information, but the partials of vec(A) are much easier to implement in a computer. Temporarily treating Λ_{ij} as a vector of dummy variables, higher-order derivatives of $G_{ij,m}$ are given by

(3.9)
$$G_{ij,m}^{(k)}(\Lambda_{ij}) = \frac{\partial \text{vec}\left(G_{ij,m}^{(k-1)}(\Lambda_{ij})\right)}{\partial \Lambda_{ij}^{\top}} \in \mathbb{R}^{(n_i + n_j)^{(k-1)} \times (n_i + n_j)}, \quad k \ge 1.$$

We replace $\Delta \Xi_{ij}$ in (3.8) with the Floquet eigenfunction expansions (3.7) and replace each ψ_i with its expansion (3.6). With these substitutions in place, we collect the expansion of G_{ij} in powers of ε . The notation becomes cumbersome, so we summarize this step by writing

$$G_{ij}(\theta_{i}, \psi_{i}, \theta_{j}, \psi_{j}) = K_{ij}^{(0)}(\theta_{i}, \theta_{j})$$

$$+ \varepsilon K_{ij}^{(1)} \left(\theta_{i}, \theta_{j}, p_{i}^{(1)}, p_{j}^{(1)}\right)$$

$$+ \varepsilon^{2} K_{ij}^{(2)} \left(\theta_{i}, \theta_{j}, p_{i}^{(1)}, p_{i}^{(2)}, p_{j}^{(1)}, p_{j}^{(2)}\right)$$

$$+ \varepsilon^{3} K_{ij}^{(3)} \left(\theta_{i}, \theta_{j}, p_{i}^{(1)}, p_{i}^{(2)}, p_{i}^{(3)}, p_{j}^{(1)}, p_{j}^{(2)}, p_{j}^{(3)}\right)$$

$$+ \cdots .$$

The $K^{(\ell)}$ functions contain the collected Floquet eigenfunctions and the partial derivatives of G_{ij} for each order $O(\varepsilon^{\ell})$. We compute more explicit forms of $K_{ij}^{(\ell)}$ in Appendix C for use in some explicit calculations in section 4.1. It is straightforward to verify using a symbolic package that the function $K^{(k)}$ only depends on terms $p_i^{(\ell)}$, $p_j^{(\ell)}$ for $\ell \leq k$. For additional details, we refer the reader to our code repository [45], where we implement SymPy to automate the collection of symbolic terms [37].

Note that the ε -expansion of Q_i is just as straightforward to calculate using the above method. We summarize the expansion of Q_i by writing

$$Q_{i}(\theta_{i}, \psi_{i}) = Q_{i}^{(0)}(\theta_{i}) + \varepsilon Q_{i}^{(1)}\left(\theta_{i}, p_{i}^{(1)}\right) + \varepsilon^{2} Q_{i}^{(2)}\left(\theta_{i}, p_{i}^{(1)}, p_{i}^{(2)}\right) + \varepsilon^{3} Q_{i}^{(3)}\left(\theta_{i}, p_{i}^{(1)}, p_{i}^{(2)}, p_{i}^{(3)}\right) + \cdots$$

More explicit forms for $Q_i^{(\ell)}$ are also in Appendix C, and have almost the same form as the expression for $K_{ij}^{(\ell_1,\ell_2)}$. These more explicit terms will likewise be used in the section 4.1 calculations.

3.2. Elimination of isostable coordinates. While we now have all the necessary expansions in ε to rewrite the phase-amplitude equations (3.2) in powers of ε , there remain two variables for each oscillator: θ_i and ψ_i . Thus, some work remains to reduce the system to a single phase variable. We proceed with the method suggested by [69, 50], by deriving and solving linear equations for each term $p_i^{(k)}$ in the expansion of ψ_i (3.6). We state two key assumptions before proceeding.

Assumption 1. There exists a sufficient separation of timescales between $\hat{\theta}_i$ and θ_i (where $\hat{\theta}_i = \theta_i - t$), such that $\hat{\theta}_i$ can be treated as constant in time integrals. To be more precise, we assume that the averaged dynamics of $\hat{\theta}$ are relatively slow compared to t.

Assumption 2. First-order averaging is sufficient to capture nonlinear effects well beyond first order in ε . This assumption implies some upper bound on ε , but we will utilize higher-order averaging from, e.g., [31, 32] in future work if needed.

We begin by subtracting the moving frame and letting $\hat{\theta}_i = \theta_i - t$. Then the phase-amplitude equations (3.2) become

(3.11)

$$\dot{\hat{\theta}}_i = \delta \mathcal{Z}_i(\hat{\theta}_i + t, \psi_i) \cdot Q_i(\hat{\theta}_i + t, \psi_i) + \varepsilon \sum_{i=1}^N a_{ij} \mathcal{Z}_i(\hat{\theta}_i + t, \psi_i) \cdot G_{ij}(\hat{\theta}_i + t, \psi_i, \hat{\theta}_j + t, \psi_j),$$

(3.12)

$$\dot{\psi}_i = \kappa_i \psi_i + \delta \mathcal{I}_i(\hat{\theta}_i + t, \psi_i) \cdot Q_i(\hat{\theta}_i + t, \psi_i) + \varepsilon \sum_{j=1}^N a_{ij} \mathcal{I}_i(\hat{\theta}_i + t, \psi_i) \cdot G_{ij}(\hat{\theta}_i + t, \psi_i, \hat{\theta}_j + t, \psi_j).$$

Substituting the expansion $\psi_i(t) = \varepsilon p_i^{(1)}(t) + \varepsilon^2 p_i^{(2)}(t) + \varepsilon^3 p_i^{(3)}(t) + \cdots$ into (3.12) yields a hierarchy of ODEs in powers of ε . The left-hand side consists of straightforward time derivatives:

$$\dot{\psi}_i = \varepsilon \frac{d}{dt} p_i^{(1)} + \varepsilon^2 \frac{d}{dt} p_i^{(2)} + \varepsilon^3 \frac{d}{dt} p_i^{(3)} + \cdots,$$

and the right-hand side includes many cross-multiplication terms (not all ψ_i are shown expanded in ε for brevity):

$$\kappa_{i}\psi_{i} + \delta\mathcal{I}_{i}(\hat{\theta}_{i} + t, \psi_{i}) \cdot Q_{i}(\hat{\theta}_{i} + t, \psi_{i}) + \varepsilon \sum_{j=1}^{N} a_{ij}\mathcal{I}_{i}(\hat{\theta}_{i} + t, \psi_{i}) \cdot G_{ij}(\hat{\theta}_{i} + t, \psi_{i}, \hat{\theta}_{j} + t, \psi_{j})$$

$$= \kappa_{i} \left[\varepsilon p_{i}^{(1)}(t) + \varepsilon^{2} p_{i}^{(2)}(t) + \cdots \right]$$

$$+ \delta \left\{ \left[I_{i}^{(0)}(\hat{\theta}_{i} + t) + \psi_{i} I_{i}^{(1)}(\hat{\theta}_{i} + t) + \psi_{i}^{2} I_{i}^{(2)}(\hat{\theta}_{i} + t) + \cdots \right]$$

$$\cdot \left[Q_{i}^{(0)}(\theta_{i}) + \varepsilon Q_{i}^{(1)}(\theta_{i}, p_{i}^{(1)}) + \varepsilon^{2} Q_{i}^{(2)}(\theta_{i}, p_{i}^{(1)}, p_{i}^{(2)}) + \varepsilon^{3} Q_{i}^{(3)}(\theta_{i}, p_{i}^{(1)}, p_{i}^{(2)}, p_{i}^{(3)}) + \cdots \right] \right\}$$

$$+ \varepsilon^{3} Q_{i}^{(3)}(\theta_{i}, p_{i}^{(1)}, p_{i}^{(2)}, p_{i}^{(3)}) + \cdots \right]$$

$$+ \varepsilon \sum_{j=1}^{N} a_{ij} \left\{ \left[I_{i}^{(0)}(\hat{\theta}_{i} + t) + \psi_{i} I_{i}^{(1)}(\hat{\theta}_{i} + t) + \psi_{i}^{2} I_{i}^{(2)}(\hat{\theta}_{i} + t) + \cdots \right]$$

$$\cdot \left[K_{ij}^{(0)}(\hat{\theta}_{i} + t, \hat{\theta}_{j} + t) + \varepsilon K_{ij}^{(1)}(\hat{\theta}_{i} + t, \hat{\theta}_{j} + t, p_{i}^{(1)}, p_{j}^{(1)}) + \varepsilon^{2} K_{ij}^{(2)}(\hat{\theta}_{i} + t, \hat{\theta}_{j} + t, p_{i}^{(1)}, p_{i}^{(2)}, p_{j}^{(1)}, p_{j}^{(2)}) + \varepsilon^{3} K_{ij}^{(3)}(\hat{\theta}_{i} + t, \hat{\theta}_{j} + t, p_{i}^{(1)}, p_{i}^{(2)}, p_{i}^{(3)}, p_{j}^{(1)}, p_{j}^{(2)}, p_{j}^{(3)}) + \cdots \right] \right\}.$$

Writing $\delta = \varepsilon \delta/\varepsilon \equiv \varepsilon b$ and recollecting in powers of ε yields a hierarchy of scalar ODEs, which we show up to order ε^3 in (3.13). We suppress the explicit θ_i -, θ_j -dependence of $p_i^{(k)}$, $I^{(k)}$, and $K^{(k)}$.

(3.13)

$$O(\varepsilon): \frac{dp_i^{(1)}}{dt} = \kappa_i p_i^{(1)} + bI_i^{(0)} \cdot Q_i^{(0)} + \sum_{j=1}^N a_{ij} I_i^{(0)} \cdot K_{ij}^{(0)},$$

$$O(\varepsilon^2): \frac{dp_i^{(2)}}{dt} = \kappa_i p_i^{(2)} + bp_i^{(1)} I_i^{(1)} \cdot Q_i^{(0)} + bI_i^{(0)} \cdot Q_i^{(1)} + \sum_{j=1}^N a_{ij} \left(I_i^{(0)} \cdot K_{ij}^{(1)} + p_i^{(1)} I_i^{(1)} \cdot K_{ij}^{(0)} \right),$$

$$\begin{split} O(\varepsilon^3) : \frac{dp_i^{(3)}}{dt} &= \kappa_i p_i^{(3)} + b p_i^{(2)} I_i^{(1)} + b \left(p_i^{(1)} \right)^2 I_i^{(2)} + b p_i^{(1)} I_i^{(1)} \cdot Q_i^{(1)} + b I_i^{(0)} \cdot Q_i^{(2)} \\ &+ \sum_{j=1}^N a_{ij} \left(I_i^{(0)} \cdot K_{ij}^{(2)} + p_i^{(1)} I_i^{(1)} \cdot K_{ij}^{(1)} + p_i^{(2)} I_i^{(1)} \cdot K_{ij}^{(0)} + \left(p_i^{(1)} \right)^2 I_i^{(2)} \cdot K_{ij}^{(0)} \right), \end{split}$$

Each ODE is a first-order inhomogeneous differential equation with a forcing term that depends on lower-order solutions and is thus solvable. To demonstrate our calculations concretely, we begin by explicitly solving the lowest-order term $p_i^{(1)}$. Throughout the calculations in the remainder of this section, we will often use θ_i in place of $\hat{\theta}_i + t$.

With all of its dependencies, the lowest-order equation is written as

$$\frac{dp_i^{(1)}}{dt}(t) = \kappa_i p_i^{(1)}(t) + bI_i^{(0)}(\theta_i) \cdot Q_i^{(0)}(\theta_i) + \sum_{j_1=1}^N a_{ij_1} I_i^{(0)}(\theta_i) \cdot K_{ij_1}^{(0)}(\theta_i, \theta_{j_1}).$$

Applying the integrating factor method, we arrive at the solution,

$$p_i^{(1)}(t) = \int_{t_0}^t e^{\kappa_i(t-s)} \left(bI_i^{(0)}(\hat{\theta}_i + s) \cdot Q_i^{(0)}(\hat{\theta}_i + s) + \sum_{j_1=1}^N a_{ij_1} I_i^{(0)}(\hat{\theta}_i + s) \cdot K_{ij_1}^{(0)}(\hat{\theta}_i + s, \hat{\theta}_{j_1} + s) \right) ds + e^{\kappa_i t} C,$$

where C is a constant of integration. To discard transients, we ignore the constant of integration and take $t_0 \to -\infty$. Then, with the change of variables $s \to t - s$, the equation becomes

(3.14)
$$p_i^{(1)}(t) = bq_i(\theta_i) + \sum_{j_1=1}^N a_{ij_1} g_{ij_1}(\theta_i, \theta_{j_1}),$$

where

$$q_i(\xi) = \int_0^\infty e^{\kappa_i s} I_i^{(0)}(\xi - s) \cdot Q_i^{(0)}(\xi - s) \, \mathrm{d}s,$$
$$g_{ij}(\xi_1, \xi_2) = \int_0^\infty e^{\kappa_i s} I_i^{(0)}(\xi_1 - s) \cdot K_{ij}^{(0)}(\xi_1 - s, \xi_2 - s) \, \mathrm{d}s$$

are functions that may be precomputed. We use (3.14) to solve for $p_i^{(2)}$, yielding, with appropriate rearrangement,

(3.15)
$$p_i^{(2)}(t) = b \sum_{j_1} q_{ij_1}(\theta_i, \theta_{j_1}) + \sum_{j_1, j_2} g_{ij_1j_2}(\theta_i, \theta_{j_1}, \theta_{j_2}),$$
Heterogeneity Coupling

where each function q_{ij_1} ($g_{ij_1j_2}$) is distinguishable from q_i (g_{ij_1}) by the number of indices. We find that the heterogeneous term contains two-body interactions and the coupling term

contains three-body interactions. While our goal is not necessarily to enumerate every term explicitly, we show the forcing function terms for $p_i^{(2)}$ term by term (and obtain more explicit equations for q_{ij_1} and $g_{ij_1j_2}$ in (3.16)):

$$\begin{split} bp_i^{(1)}I_i^{(1)} \cdot Q_i^{(0)} &= b^2q_iI_i^{(1)} \cdot Q_i^{(0)} + b\sum_{j_1}a_{ij_1}g_{ij_1}I_i^{(1)} \cdot Q_i^{(0)}, \\ bI_i^{(0)} \cdot Q_i^{(1)} &= bI_i^{(0)} \cdot u_i^{(1)} \left[bq_i + \sum_{j_1}a_{ij_1}g_{ij_1}\right] \\ &= b^2I_i^{(0)} \cdot u_i^{(1)}q_i + b\sum_{j_1}a_{ij_1}g_{ij_1}I_i^{(0)} \cdot u_i^{(1)}, \\ I_i^{(0)} \cdot K_{ij}^{(1)} &\equiv I_i^{(0)} \cdot \left[p_i^{(1)}v_{ij}^{(1,0)} + p_j^{(1)}v_{ij}^{(0,1)}\right] \\ &= I_i^{(0)} \cdot \left[bq_i + \sum_{j_1}a_{ij_1}g_{ij_1}\right]v_{ij}^{(1,0)} + \left[b_jq_j + \sum_{j_1}a_{jj_1}g_{jj_1}\right]v_{ij}^{(0,1)}\right] \\ &= I_i^{(0)} \cdot \left[bq_iv_{ij}^{(1,0)} + b_jq_jv_{ij}^{(0,1)}\right] + I_i^{(0)} \cdot \sum_{j_1}\left[a_{ij_1}g_{ij_1}v_{ij}^{(1,0)} + a_{jj_1}g_{jj_1}v_{ij}^{(0,1)}\right], \\ p_i^{(1)}I_i^{(1)} \cdot K_{ij}^{(0)} &= \left[bq_i + \sum_{j_1}a_{ij_1}g_{ij_1}\right]I_i^{(1)} \cdot K_{ij}^{(0)} \\ &= bq_iI_i^{(1)} \cdot K_{ij}^{(0)} + \sum_{j_1}a_{ij_1}g_{ij_1}I_i^{(1)} \cdot K_{ij}^{(0)}. \end{split}$$

Thus, we may write (3.15) more explicitly:

$$(3.16) p_i^{(2)}(t) = b^2 q_{ij_0}(\theta_i) + b \sum_{j_1} q_{ij_1}(\theta_i, \theta_{j_1}) + \sum_{j_1} \sum_{j_2} g_{ij_1j_2}(\theta_i, \theta_{j_1}, \theta_{j_2}) + \hat{g}_{ij_1j_2}(\theta_i, \theta_{j_1}, \theta_{j_2}),$$

where

$$q_{ij_0}(\xi) = \int_0^\infty e^{\kappa_i s} \left[q_i(\xi - s) I_i^{(1)}(\xi - s) \cdot Q_i^{(0)}(\xi - s) + q_i(\xi - s) I_i^{(0)}(\xi - s) \cdot u_i^{(1)}(\xi - s) \right] ds,$$

$$q_{ij_1}(\xi_1, \xi_2) = \int_0^\infty e^{\kappa_i s} \left[q_i(\xi_1 - s) I_i^{(0)}(\xi_1 - s) \cdot v_{ij_1}^{(1,0)}(\xi_1 - s, \xi_2 - s) + q_{j_1}(\xi_2 - s) I_i^{(0)}(\xi_1 - s) \cdot v_{ij_1}^{(0,1)}(\xi_1 - s, \xi_2 - s) + q_i(\xi_1 - s) I_i^{(1)}(\xi_1 - s) \cdot K_{ij_1}^{(0)}(\xi_1 - s, \xi_2 - s) + g_{ij_1}(\xi_1 - s, \xi_2 - s) I_i^{(1)}(\xi_1 - s) \cdot Q_i^{(0)}(\xi_1 - s) + g_{ij_1}(\xi_1 - s, \xi_2 - s) I_i^{(0)}(\xi_1 - s) \cdot u_i^{(1)}(\xi_1 - s) \right] ds,$$

$$g_{ij_1j_2}(\xi_1, \xi_2, \xi_3) = \int_0^\infty e^{\kappa_i s} \left[g_{ij_2}(\xi_1 - s, \xi_3 - s) I_i^{(0)}(\xi_1 - s) \cdot v_{ij_1}^{(1,0)}(\xi_1 - s, \xi_2 - s) + g_{ij_2}(\xi_1 - s, \xi_3 - s) I_i^{(1)}(\xi_1 - s) \cdot K_{ij_1}^{(0)}(\xi_1 - s, \xi_2 - s) \right] ds,$$

$$\hat{g}_{ij_1j_2}(\xi_1, \xi_2, \xi_3) = \int_0^\infty e^{\kappa_i s} g_{j_1j_2}(\xi_2 - s, \xi_3 - s) I_i^{(0)}(\xi_1 - s) \cdot v_{ij_1}^{(0,1)}(\xi_1 - s, \xi_2 - s) ds.$$

Even more explicit terms that include pairwise coupling terms a_{ij} are shown in [42, Appendix C].

Note that b increases in power for each new term; thus we require $b \leq 1$ for arbitrarily highorder expansions, which is equivalent to the condition that the overall strength of heterogeneity must be less than or equal to the overall coupling strength ($\delta \leq \varepsilon$). This condition is not restrictive, however, because we tend not to take arbitrarily high expansions, and coupling may be weakened relative to heterogeneity by adjusting the coupling constants a_{ij} .

We continue these calculations for each order k to obtain solutions of the same form as (3.15):

$$p_i^{(k)}(t) = b \sum_{\ell=1}^k \sum_{j_1, \dots, j_{\ell-1}} q_{ij_1 \dots j_{\ell-1}}(\theta_i, \theta_{j_1}, \dots, \theta_{j_{\ell-1}}) + \underbrace{\sum_{\ell=1}^k \sum_{j_1, \dots, j_\ell} g_{ij_1 \dots j_\ell}(\theta_i, \theta_{j_1}, \dots, \theta_{j_\ell})}_{\text{Coupling}}.$$

The maximum number of indices j_1, \ldots, j_k is N-1, because we use one index for oscillator i and there are N oscillators. Naturally, higher-order terms for $k \geq N$ do not introduce additional higher-order interactions, but may improve the accuracy of the expansion.

Now that we have expressed each $p_i^{(k)}$ in terms of phase, effectively eliminating the isostable equation, we turn to deriving a phase difference equation.

3.3. Phase difference equation. We expand the phase equation (3.11) in ε (where again, for brevity, not all ψ_i are shown expanded in ε):

$$\begin{split} \dot{\hat{\theta}}_{i} &= \delta \mathcal{Z}_{i}(\hat{\theta}_{i} + t, \psi_{i}) \cdot Q_{i}(\hat{\theta}_{i} + t, \psi_{i}) + \varepsilon \sum_{j=1}^{N} a_{ij} \mathcal{Z}_{i}(\hat{\theta}_{i} + t, \psi_{i}) \cdot G_{ij}(\hat{\theta}_{i} + t, \hat{\theta}_{j} + t) \\ &= \delta \left\{ \left[Z_{i}^{(0)}(\hat{\theta}_{i} + t) + \psi_{i} Z_{i}^{(1)}(\hat{\theta}_{i} + t) + \psi_{i}^{2} Z_{i}^{(2)}(\hat{\theta}_{i} + t) + \cdots \right] \right. \\ & \left. \cdot \left[Q_{i}^{(0)}(\theta_{i}) + \varepsilon Q_{i}^{(1)} \left(\theta_{i}, p_{i}^{(1)} \right) + \varepsilon^{2} Q_{i}^{(2)} \left(\theta_{i}, p_{i}^{(1)}, p_{i}^{(2)} \right) \right. \\ & \left. + \varepsilon^{3} Q_{i}^{(3)} \left(\theta_{i}, p_{i}^{(1)}, p_{i}^{(2)}, p_{i}^{(3)} \right) + \cdots \right] \right\} \\ & \left. + \varepsilon \sum_{j=1}^{N} a_{ij} \left[Z_{i}^{(0)} + \psi_{i} Z_{i}^{(1)} + \psi_{i}^{2} Z_{i}^{(2)} + \cdots \right] \cdot \left[K_{ij}^{(0)} + \varepsilon K_{ij}^{(1)} + \varepsilon^{2} K_{ij}^{(2)} + \cdots \right]. \end{split}$$

Substituting the expansion for ψ_i and collecting in powers of ε yields a virtually identical right-hand side as (3.13) with Z in place of I:

$$\begin{split} \dot{\hat{\theta}}_{i} &= \varepsilon \left[b Z_{i}^{(0)} \cdot Q_{i}^{(0)} + \sum_{j=1}^{N} a_{ij} Z_{i}^{(0)} \cdot K_{ij}^{(0)} \right] \\ &+ \varepsilon^{2} \left[b p_{i}^{(1)} Z_{i}^{(1)} \cdot Q_{i}^{(0)} + b Z_{i}^{(0)} \cdot Q_{i}^{(1)} + \sum_{j=1}^{N} a_{ij} \left(Z_{i}^{(0)} \cdot K_{ij}^{(1)} + p_{i}^{(1)} Z_{i}^{(1)} \cdot K_{ij}^{(0)} \right) \right] \\ &+ \varepsilon^{3} \left[b p_{i}^{(2)} I_{i}^{(1)} + b \left(p_{i}^{(1)} \right)^{2} I_{i}^{(2)} + b p_{i}^{(1)} I_{i}^{(1)} \cdot Q_{i}^{(1)} + b I_{i}^{(0)} \cdot Q_{i}^{(2)} \right. \\ &+ \left. \sum_{j=1}^{N} a_{ij} \left(Z_{i}^{(0)} \cdot K_{ij}^{(2)} + p_{i}^{(1)} Z_{i}^{(1)} \cdot K_{ij}^{(1)} + p_{i}^{(2)} Z_{i}^{(1)} \cdot K_{ij}^{(0)} + \left(p_{i}^{(1)} \right)^{2} Z_{i}^{(2)} \cdot K_{ij}^{(0)} \right) \right] \\ \vdots \\ \vdots \\ \end{split}$$

This differential equation is a system of nonautonomous ODEs for the phase dynamics of each oscillator.

We now use averaging theory to transform this nonautonomous system (3.17) into an autonomous system. Again, for concreteness, we examine the first few terms of the right-hand side. The averaged order $O(\varepsilon)$ dynamics satisfy

$$b\tilde{q}_i + \sum_{j_1=1}^N a_{ij_1} \mathcal{H}_{ij_1}^{(1)}(\theta_{j_1} - \theta_i),$$

where

$$\tilde{q}_i = \frac{1}{T} \int_0^T Z_i^{(0)}(s) \cdot Q_i^{(0)}(s) \, \mathrm{d}s,$$

$$\mathcal{H}_{ij_1}(\xi) = \frac{1}{T} \int_0^T Z_i^{(0)}(s) \cdot K_{ij_1}^{(0)}(s, \xi + s) \, \mathrm{d}s.$$

The $\mathcal{H}_{ij_1}^{(1)}$ term is identical to the classic weak coupling theory for N oscillators (see, e.g., [17, Chapter 8, eq. (8.38)]). The next order $O(\varepsilon^2)$ terms are

$$\begin{split} bp_i^{(1)}Z_i^{(1)}\cdot Q_i^{(0)} &= b^2\tilde{q}_iZ_i^{(1)}\cdot Q_i^{(0)} + b\sum_{j_1}a_{ij_1}g_{ij_1}Z_i^{(1)}\cdot Q_i^{(0)},\\ bZ_i^{(0)}\cdot Q_i^{(1)} &= bZ_i^{(0)}\cdot u_i^{(0)}\left[b\tilde{q}_i + \sum_{j_1}a_{ij_1}g_{ij_1}\right]\\ &= b^2Z_i^{(0)}\cdot u_i^{(0)}\tilde{q}_i + b\sum_i a_{ij_1}g_{ij_1}Z_i^{(0)}\cdot u_i^{(0)}, \end{split}$$

$$\begin{split} Z_i^{(0)} \cdot K_{ij}^{(1)} &\equiv Z_i^{(0)} \cdot \left[p_i^{(1)} v_{ij}^{(1,0)} + p_j^{(1)} v_{ij}^{(0,1)} \right] \\ &= Z_i^{(0)} \cdot \left[\left[b \tilde{q}_i + \sum_{j_1} a_{ij_1} g_{ij_1} \right] v_{ij}^{(1,0)} + \left[b q_j + \sum_{j_1} a_{jj_1} g_{jj_1} \right] v_{ij}^{(0,1)} \right] \\ &= b Z_i^{(0)} \cdot \left[\tilde{q}_i v_{ij}^{(1,0)} + q_j v_{ij}^{(0,1)} \right] + Z_i^{(0)} \cdot \sum_{j_1} a_{ij_1} g_{ij_1} v_{ij}^{(1,0)} + a_{jj_1} g_{jj_1} v_{ij}^{(0,1)}, \\ p_i^{(1)} Z_i^{(1)} \cdot K_{ij}^{(0)} &= \left[b \tilde{q}_i + \sum_{j_1} a_{ij_1} g_{ij_1} \right] Z_i^{(1)} \cdot K_{ij}^{(0)} \\ &= b \tilde{q}_i Z_i^{(1)} \cdot K_{ij}^{(0)} + \sum_{j_1} a_{ij_1} g_{ij_1} Z_i^{(1)} \cdot K_{ij}^{(0)}. \end{split}$$

Thus, the second-order term is given by

$$b\sum_{j_1} \tilde{q}_{ij_1}(\hat{\theta}_{j_1} - \hat{\theta}_i) + \sum_{j_1, j_2} \mathcal{H}_{ij_1j_2}(\hat{\theta}_{j_1} - \hat{\theta}_i, \hat{\theta}_{j_2} - \hat{\theta}_i),$$

where

$$\begin{split} b \sum_{j_1} \tilde{q}_{ij_1}(\xi) &= \frac{b^2}{T} \int_0^T \tilde{q}_i(s) Z_i^{(1)}(s) \cdot Q_i^{(0)}(s) \, \mathrm{d}s + \frac{b^2}{T} \int_0^T \tilde{q}_i(s) u_i^{(1)}(s) \cdot Q_i^{(0)}(s) \, \mathrm{d}s \\ &+ \sum_{j_1} \frac{b}{T} \int_0^T \tilde{q}_i(s) Z_i^{(0)}(s) \cdot v_{ij_1}^{(1,0)}(s,\xi+s) \, \mathrm{d}s \\ &+ \sum_{j_1} \frac{b}{T} \int_0^T \tilde{q}_i(s) Z_i^{(0)}(s) \cdot v_{ij_1}^{(0,1)}(s,\xi+s) \, \mathrm{d}s \\ &+ \sum_{j_1} \frac{b}{T} \int_0^T \tilde{q}_i(s) Z_i^{(1)}(s) \cdot K_{ij_1}^{(0)}(s,\xi+s) \, \mathrm{d}s \\ &+ \sum_{j_1} \frac{ba_{ij_1}}{T} \int_0^T Z_i^{(1)}(s) \cdot Q_i^{(0)}(s) g_{ij_1}(s,\xi+s) \, \mathrm{d}s \\ &+ \sum_{j_1} \frac{ba_{ij_1}}{T} \int_0^T Z_i^{(1)}(s) \cdot Q_i^{(0)}(s) g_{ij_1}(s,\xi+s) \, \mathrm{d}s \\ &+ \sum_{j_1} \frac{ba_{ij_2}}{T} \int_0^T Z_i^{(0)}(s) \cdot v_{ij_1}^{(1,0)}(s,\xi+s) g_{ij_2}(s,\xi+s) \, \mathrm{d}s \\ &+ \sum_{j_1,j_2} \frac{a_{ij_2}}{T} \int_0^T Z_i^{(0)}(s) \cdot v_{ij_1}^{(1,0)}(s,\xi_1+s) g_{j_1j_2}(\xi_1+s,\xi_2+s) \, \mathrm{d}s \\ &+ \sum_{j_1,j_2} \frac{a_{ij_2}}{T} \int_0^T Z_i^{(0)}(s) \cdot K_{ij_1}^{(0)}(s,\xi_1+s) g_{ij_2}(s,\xi_2+s) \, \mathrm{d}s. \end{split}$$

Three-body interactions are apparent, as is the existence of interactions between coupling and heterogeneity. These terms, with b = 0, are the second-order interaction terms from [69].

A careful examination of these explicit terms may be of interest in future work, but we collapse them into single functions and continue these calculations with the aid of a symbolic package up to some chosen order k:

$$\dot{\hat{\theta}}_{i} = b \underbrace{\sum_{\ell=1}^{k} \varepsilon^{\ell} \sum_{j_{1}, \dots, j_{\ell-1}} \tilde{q}_{ij_{1} \dots j_{\ell-1}}^{(k)}(\hat{\theta}_{i}, \hat{\theta}_{j_{1}}, \dots, \hat{\theta}_{j_{\ell-1}})}_{\text{Heterogeneity}} + \underbrace{\sum_{\ell=1}^{k} \varepsilon^{\ell} \sum_{j_{1}, \dots, j_{\ell}} \mathcal{H}_{ij_{1} \dots j_{\ell}}^{(k)}(\hat{\theta}_{i}, \hat{\theta}_{j_{1}}, \dots, \hat{\theta}_{j_{\ell}})}_{\text{Coupling}}.$$

Defining $\phi_i = \hat{\theta}_i - \hat{\theta}_1$, we arrive at the phase difference equation,

(3.18)
$$\dot{\phi}_{i} = b \sum_{\ell=1}^{k} \varepsilon^{\ell} \sum_{j_{1}, \dots, j_{\ell-1}} \left[\tilde{q}_{i, j_{1}, \dots, j_{\ell-1}}^{(\ell)} (\phi_{j_{1}} - \phi_{i}, \dots, \phi_{j_{\ell-1}} - \phi_{i}) - \tilde{q}_{1, j_{1}, \dots, j_{\ell-1}}^{(\ell)} (\phi_{j_{1}}, \dots, \phi_{j_{\ell-1}}) \right] + \sum_{\ell=1}^{k} \varepsilon^{\ell} \sum_{j_{1}, \dots, j_{\ell}} \left[\mathcal{H}_{i, j_{1}, \dots, j_{\ell}}^{(\ell)} (\phi_{j_{1}} - \phi_{i}, \dots, \phi_{j_{\ell}} - \phi_{i}) - \mathcal{H}_{1, j_{1}, \dots, j_{\ell}}^{(\ell)} (\phi_{j_{1}}, \dots, \phi_{j_{\ell}}) \right]$$

for i = 2, ..., N. This equation is a generalized version of the two-body interactions in [50] and a generalization beyond the second-order coupling terms in [69]. Since we will not examine particular terms in the inner summation, we rewrite the right-hand side as a single \mathcal{H} function for each oscillator i and order ℓ for notational convenience:

(3.19)
$$\dot{\phi}_i = \sum_{\ell=1}^k \varepsilon^{\ell} \left[b \tilde{q}_i^{(\ell)}(\phi_2, \dots, \phi_N) + \mathcal{H}_i^{(\ell)}(\phi_2, \dots, \phi_N) \right], \quad i = 2, \dots, N.$$

Remarks.

- At order k and above, heterogeneity contributes (k-1)-body interactions (heterogeneity contributes a constant term in the lowest-order term).
- The choice of additive, linear heterogeneity in the original system (3.1) yields additive, linear heterogeneity in the reduced dynamics (3.19). This choice is not strictly necessary. While we do not require oscillators to have identical or even similar vector fields, consider for the sake of example that we have a system of identical neural oscillators where oscillator i has one heterogeneous parameter c_i in the dynamics of some gating variable X,

$$X_{\infty}(V_i; c_i) = 1/(1 + \exp((V_i + c_i))),$$

while all other oscillators $j \neq i$ have $c_i = 0$. Such a system can be transformed into the current framework by taking a Taylor expansion from the parameter value(s) $c^* = 0$ at which all oscillator periods are the same. Then,

$$X_{\infty}(V_i; c_i) = X_{\infty}(V_i; c^*) + (c_i - c^*)X_1 + (c_i - c^*)^2 X_2 + \cdots,$$

where X_i are the higher-order terms in the Taylor expansion. Taking $\delta = c_i$, higher-order δ terms may be included in the formulation.

- While we simplified our assumptions to include only one heterogeneous parameter, a generalization to multiple heterogeneous parameters is straightforward. Using the same calculations as above, if c^* is an arbitrary heterogeneous term where all oscillators have equal period, then we can compute the same Taylor expansion as above for each oscillator and obtain the parameter $\delta_i = |c_i c^*|$ for each i. Note that there is no restriction on the number of heterogeneous parameters per oscillator, so long as there exist parameter values where all oscillator periods are equal.
- Heterogeneity and asymmetry may induce interesting dynamics that will be considered in future work, but we disregard heterogeneous effects for the remainder of the paper to focus on the primary goal of confirming that the proposed N-body phase reduction is valid in the simple case of identical oscillators with homogeneous coupling.
- The phase difference equation may also be derived by using the averaged isostable expansion terms, $\bar{p}_i^{(k)}$, which, like $\hat{\theta}_i$, tend to have a slowly varying mean, even when ε is not arbitrarily small. The average term $\bar{p}_i^{(k)}$ is useful because it only depends on the relatively slow phases $\hat{\theta}_i, \hat{\theta}_j$, so it may be moved out of time integrals, greatly simplifying calculations. We perform this type of averaging in the thalamic model in section 5.
- **4. Complex Ginzburg–Landau model.** We now apply the proposed method to a set of three globally coupled complex Ginzburg–Landau (CGL) models, where the coupling is diffusive and homogeneous. The ODE form of this model has been studied extensively [69, 50], making it an ideal preliminary test for our results. Let $X_i = (x_i, y_i)^{\top}$ and N = 3. The network is given by

$$\dot{X}_i = F(X_i) + \sum_{j=1}^3 a_{ij} G(X_i, X_j),$$

where

$$F(X_i) = \begin{pmatrix} \sigma x_i (1 - R_i) - y_i (1 + \rho(R_i - 1)) \\ \sigma y_i (1 - R_i) + x_i (1 + \rho(R_i - 1)) \end{pmatrix}, \quad G(X_i, X_j) = \begin{pmatrix} (x_j - x_i) - d(y_j - y_i) \\ (y_j - y_i) + d(x_j - x_i) \end{pmatrix},$$

and $R_i = x_i^2 + y_i^2$. We assume all-to-all coupling without self coupling, so that pairwise terms a_{ij} are given by

$$a_{ij} = \begin{cases} 1/N & \text{if } i \neq j, \\ 0 & \text{else.} \end{cases}$$

It is straightforward to verify that the Floquet exponent for this system is given by $\kappa = -2\sigma$, where the Floquet multiplier κ no longer has a subscript because all oscillators are identical in this example.

4.1. Explicit calculations. The g, Z, and I functions of the CGL model each have only one (the first) nontrivial mode. To make explicit calculations, we write these functions in complex Fourier form,

$$\begin{split} g_i^{(k)}(\theta_i) &= \left[\begin{array}{c} a_g^{(k)} \exp(\mathrm{i}\theta_i) + \mathrm{c.c.} \\ b_g^{(k)} \exp(\mathrm{i}\theta_i) + \mathrm{c.c.} \end{array} \right], \\ Z_i^{(k)}(\theta_i) &= \left[\begin{array}{c} a_Z^{(k)} \exp(\mathrm{i}\theta_i) + \mathrm{c.c.} \\ b_Z^{(k)} \exp(\mathrm{i}\theta_i) + \mathrm{c.c.} \end{array} \right], \\ I_i^{(k)}(\theta_i) &= \left[\begin{array}{c} a_I^{(k)} \exp(\mathrm{i}\theta_i) + \mathrm{c.c.} \\ b_I^{(k)} \exp(\mathrm{i}\theta_i) + \mathrm{c.c.} \end{array} \right], \end{split}$$

where $a_X^{(k)}, b_X^{(k)} \in \mathbb{C}$, $X \in \{g, Z, I\}$, and "c.c." stands for "complex conjugate." We use the upright i for imaginary numbers and keep the italicized i for indices. Note that due to symmetry, $b_X^{(k)} = -\mathrm{i} a_X^{(k)}$ for all k. The limit cycle coefficients are simply $a_L = 1/2$ and $b_L = -\mathrm{i}/2$.

By assumption, $p_i^{(0)} = 0$, so we calculate the next order term,

$$p_i^{(1)}(\hat{\theta}_1, \hat{\theta}_2, \hat{\theta}_3) = \frac{1}{3\kappa} \sum_{i=1}^{3} \left[c_1 \left(1 - e^{i(\hat{\theta}_i - \hat{\theta}_j)} \right) + \text{c.c.} \right],$$

where $c_1 = 2a_L^{(0)} \bar{a}_L(1 - id) \in \mathbb{C}$. Continuing the calculation,

$$p_{i}^{(2)}(\hat{\theta}_{1}, \hat{\theta}_{2}, \hat{\theta}_{3}) = \frac{4}{9\kappa^{2}} \sum_{j_{1}=1}^{3} \sum_{j_{2}=1}^{3} \left[c_{2}e^{i(\hat{\theta}_{i} - \hat{\theta}_{j_{1}})} \left(\Re\left(c_{1}e^{i(\hat{\theta}_{j_{1}} - \hat{\theta}_{j_{2}})}\right) - \Re(c_{1}) \right) + \text{c.c.} \right]$$

$$+ \frac{4}{9\kappa^{2}} \sum_{j_{1}=1}^{3} \sum_{j_{2}=1}^{3} \left[d_{1}e^{i(\hat{\theta}_{i} - \hat{\theta}_{j_{1}})} + d_{1}e^{i(\hat{\theta}_{i} - \hat{\theta}_{j_{2}})} + \Re(d_{2})e^{i(\hat{\theta}_{j_{1}} - \hat{\theta}_{j_{2}})}$$

$$+ d_{2}e^{i(2\hat{\theta}_{i} - \hat{\theta}_{j_{1}} - \hat{\theta}_{j_{2}})} + d_{3} + \text{c.c} \right],$$

where $d_1 = -(\Re(c_1c_2 + d_2) + d_2)$, $d_2 = c_1c_3$, $d_3 = 2c_1\Re(c_2 + c_3)$, $c_2 = a_I^{(0)}\bar{a}_g^{(1)}(1 - \mathrm{i}d)$, $c_3 = a_I^{(1)}\bar{a}_L(1 - \mathrm{i}d)$. The function \Re simply returns the real part of its input.

Remarks.

- The nontrivial Floquet exponent, κ , appears in the denominator of both $p_i^{(1)}$ and $p_i^{(2)}$. Thus, a smaller nontrivial Floquet exponent $(|\kappa| \ll 1)$, which occurs for weakly attracting limit cycles, makes the isostable coordinate contribute nontrivially to the phase dynamics. While we generically expect κ to appear implicitly in the denominator, these calculations make its appearance explicit. Indeed, the inclusion of isostable coordinates for $|\kappa|$ small is the key difference between our work and purely phase-based methods.
- The coefficient for each $p_i^{(k)}$ is of the form $1/(N\kappa)^k$ and thus may diverge for large k. Questions of convergence will be explored in future work, but we note that this issue does not appear to significantly affect the results for the relatively lower-order truncation we consider.
- Higher-order terms contain not only higher-order interactions, but also higher-order Fourier modes, e.g., $e^{i(2\hat{\theta}_i \hat{\theta}_{j_1} \hat{\theta}_{j_2})}$.

• In this example, each of the functions $p_i^{(1)}$ and $p_i^{(2)}$ depends only on phase differences, so that $p_i^{(k)}(\hat{\theta}_1+t,\hat{\theta}_2+t,\hat{\theta}_3+t)=p_i^{(k)}(\hat{\theta}_1,\hat{\theta}_2,\hat{\theta}_3)$. This pure phase dependence holds so long as $b_X^{(k)}=-\mathrm{i}a_X^{(k)}$ and the oscillators are identical—we exploit this property for the numerical results in section 4.2. (This lack of time dependence is a lucky coincidence. In general, even with identical oscillators, we expect to see additional terms that do not purely depend on phase differences.)

With the solutions $p_i^{(1)}$ and $p_i^{(2)}$ in hand, we turn to the calculation of \mathcal{H} functions.

$$\mathcal{H}_{i}^{(1)} = \frac{1}{3} \sum_{j=1}^{3} \left[\hat{c}_{1} \left(e^{i \left(\hat{\theta}_{i} - \hat{\theta}_{j} \right)} - 1 \right) + \text{c.c.} \right],$$

where $\hat{c}_1 = 2a_Z^{(0)}\bar{a}_L(1-\mathrm{i}d) \in \mathbb{C}$.

$$\begin{split} \mathcal{H}_{i}^{(2)} &= \frac{2}{9\kappa} \sum_{j_{1}=1}^{3} \sum_{j_{2}=1}^{3} \left[\hat{c}_{2} \left(\Re \left(\hat{c}_{1} e^{\mathrm{i}(\hat{\theta}_{j_{1}} - \hat{\theta}_{j_{2}})} \right) - \Re (\hat{c}_{1}) \right) + \mathrm{c.c.} \right] \\ &+ \frac{1}{9\kappa} \sum_{j_{1}=1}^{3} \sum_{j_{2}=1}^{3} \left[\hat{d}_{1} e^{\mathrm{i}(\hat{\theta}_{j_{1}} - \hat{\theta}_{i})} + \hat{d}_{1} e^{\mathrm{i}(\hat{\theta}_{j_{2}} - \hat{\theta}_{i})} + \Re (\hat{d}_{2}) e^{\mathrm{i}(\hat{\theta}_{j_{2}} - \hat{\theta}_{j_{1}})} + \hat{d}_{2} e^{\mathrm{i}(-2\hat{\theta}_{i} + \hat{\theta}_{j_{2}} + \hat{\theta}_{j_{1}})} + \hat{d}_{4} + \mathrm{c.c.} \right], \end{split}$$

where $\hat{d}_1 = (\Re(\hat{c}_1\hat{c}_2 + \hat{d}_2) + \hat{d}_2)$, $\hat{d}_2 = -\hat{c}_1\hat{c}_3$, $\hat{d}_3 = -2\hat{c}_1\Re(\hat{c}_2 + \hat{c}_3)$, $\hat{c}_2 = a_Z^{(0)}\bar{a}_g^{(1)}(1 - \mathrm{i}d)$, $\hat{c}_3 = a_Z^{(1)}\bar{a}_L(1 - \mathrm{i}d)$. While it is possible to calculate $\mathcal{H}_i^{(3)}$ explicitly, the terms are far too numerous to show here. We instead proceed numerically.

4.2. Numerical results. Numerically calculating the \mathcal{H} functions (3.19) for the CGL model is straightforward because the Nyquist frequency of the underlying functions are especially low and requires only a dozen Fourier terms at $O(\varepsilon^3)$. Using a Fourier truncation in this scenario greatly reduces the time complexity and memory requirements for the averaging calculation behind the \mathcal{H} functions (see Appendix A.1 for additional details).

We show comparisons between the full and reduced versions of the CGL model in Figure 1. The top row shows phase estimates of the full model for $\varepsilon = 0.005$ (A) and $\varepsilon = 0.06$ (C), where later shades correspond to later times (see Appendix D for more details on the phase estimation of the full model). The bottom row shows the $O(\varepsilon)$ (blue), $O(\varepsilon^2)$ (orange), and $O(\varepsilon^3)$ (black) phase models exhibiting qualitatively similar dynamics at $\varepsilon = 0.005$ (E) and $\varepsilon = 0.06$ (G), respectively. Corresponding time traces are shown to the right of each portrait, e.g., panel (B) corresponds to (A), and (F) corresponds to (E).

At $\varepsilon = 0.005$, the full model tends towards an asymptotically stable splay state when initialized near synchrony with phases $(\phi_2, \phi_3) = (0.05, 0.25)$ ((A), (B), where $\phi_i \in [0, 2\pi)$). With the same initial values, all $O(\varepsilon)$ (blue), $O(\varepsilon^2)$ (orange), and $O(\varepsilon^3)$ (black) phase models coincide with each other and with the full model as expected (E), (F). For greater values of ε , the full model splay state loses stability and the phase differences converge towards a limit cycle attractor (C), (D). Only the $O(\varepsilon^3)$ (black) phase model exhibits a similar limit cycle oscillation, while the $O(\varepsilon)$ (blue) phase model dynamics do not change, and the $O(\varepsilon^2)$

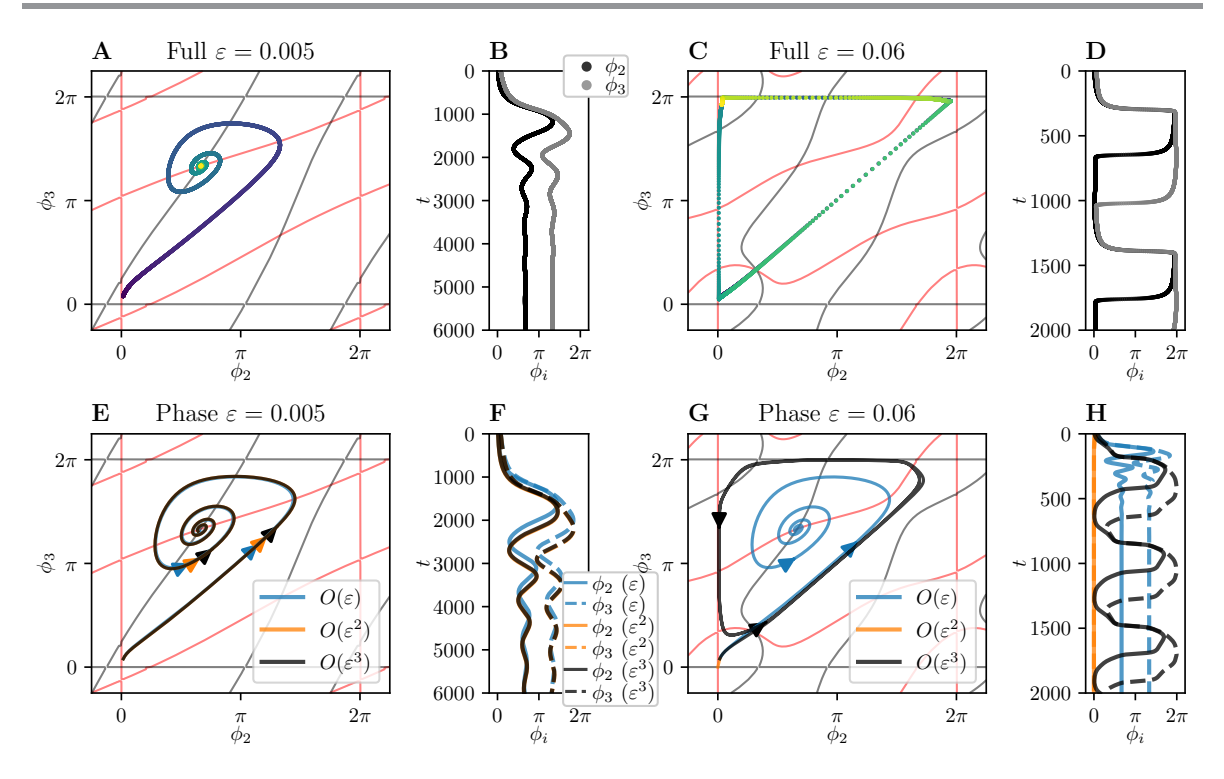


Figure 1. Comparison of the full (top row) and reduced (bottom row) CGL models. All panels show the corresponding nullclines of the $O(\varepsilon^3)$ reduced model. (A) Phase difference estimate of the full model dynamics at $\varepsilon = 0.005$. Lighter shades indicate later times. (E) The corresponding reduced models $(O(\varepsilon))$ blue, $O(\varepsilon^2)$ orange, and $O(\varepsilon^3)$ black). Arrows indicate movement in forward time. Note that all phase models coincide. (B), (F) Corresponding plots over time of the full model and reduced model, respectively. (C), (D) Full and reduced model dynamics, respectively, for $\varepsilon = 0.06$. (D), (H) Corresponding plots over time of the full and reduced models, respectively. Parameters: d = 0.9, $\sigma = 0.1$, $\rho = 0.15$. We show every hundredth time point of the full model phase estimation to reduce lag when rendering vector graphics in this document.

(orange) phase model simply converges to synchrony due to changes in the underlying basin of attraction (G), (H).

Note that even though both $O(\varepsilon^2)$ and $O(\varepsilon^3)$ terms contain three-body interactions, only the $O(\varepsilon^3)$ phase model reproduces limit cycle behavior. This example demonstrates that N-body interactions alone are not always sufficient to capture the dynamics of the original model. Additional correction terms may be necessary.

The stability of the splay state is straightforward to calculate using the reduced model because only the eigenvalues of the Jacobian matrix evaluated at the splay state $(\phi_2, \phi_3) = (2\pi/3, 4\pi/3)$ need to be known. By using the Fourier expansion of the \mathcal{H} functions, only derivatives of sinusoids are required to compute the Jacobian, and this derivative can be taken rapidly without the need for estimates such as finite differences. The result of this analysis is shown in Figure 2. The left and right panels show the real and imaginary parts of the eigenvalues, respectively. While $O(\varepsilon^2)$ (orange) does eventually lose stability, it occurs at a four-fold greater coupling strength than the full or $O(\varepsilon^3)$ models.

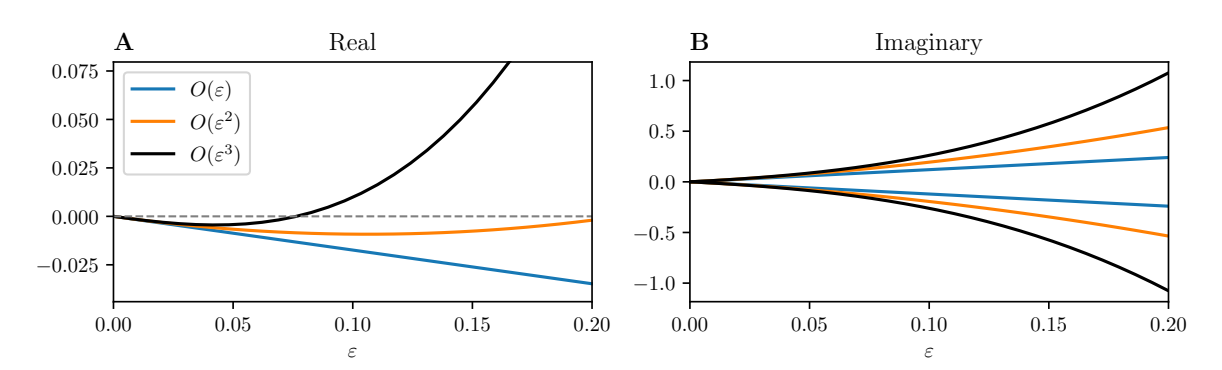


Figure 2. Real (A) and imaginary (B) parts of the eigenvalues of the Jacobian matrix evaluated at the splay state in the reduced CGL models. Blue: $O(\varepsilon)$; orange: $O(\varepsilon^2)$; black: $O(\varepsilon^3)$. The dashed line is provided for reference to highlight the loss of stability as ε increases in higher-order accuracy models. Parameters are identical to those used in Figure 1.

5. Thalamic model. We now apply the method to a set of N=3 synaptically coupled conductance-based thalamic neuron models from [56]. These results extend our previous work where we applied a strongly coupled phase reduction method for N=2 thalamic models [50].

Remark. To simplify calculating the $p_i^{(k)}$ terms for this model, we compute the averaged dynamics $\bar{p}_i^{(k)}$. Then the integral calculations for each $p_i^{(k)}$ become trivial, but the resulting solution nevertheless closely follows its original trajectory.

The thalamic model is given by the equations

$$\frac{dV_{i}}{dt} = -\left(I_{L}(V_{i}) + I_{Na}(V_{i}) + I_{K}(V_{i}) + I_{T}(V_{i}) + \frac{g_{\text{syn}}}{N} \sum_{j=1}^{N} a_{ij} w_{j} (V_{i} - E_{\text{syn}}) - I_{\text{app}}\right) / C,$$

$$\frac{dh_{i}}{dt} = (h_{\infty}(V_{i}) - h_{i}) / \tau_{h}(V_{i}),$$

$$\frac{dr_{i}}{dt} = (r_{\infty}(V_{i}) - r_{i}) / \tau_{r}(V_{i}),$$

$$\frac{dw_{i}}{dt} = \alpha(1 - w_{i}) / (1 + \exp((V_{i} - V_{T}) / \sigma_{T})) - \beta w_{i},$$

where i = 1, ..., 3, and $a_{ii} = 0$ and $a_{ij} = 1$ otherwise. Remaining equations are found in Appendix B, and all parameters are shown in Table 1. Given neuron i, the coupling term in the voltage variable V_i is given by the average excitatory effect of the synaptic variables w_j without self-coupling. The synaptic conductance parameter g_{syn} sets the overall coupling strength and is identical to the coupling strength parameter ε .

We compare the reduced and full versions of the thalamic model in Figure 3, where the parameters are chosen as in Table 1 with $E_{\rm syn}=0$ mV and $I_{\rm app}=0.8~\mu{\rm A/cm^2}$. The top row shows phase estimates of the full model for $\varepsilon=0.005$ (A) and $\varepsilon=0.027$ (C), where lighter shades correspond to later times (see Appendix D for more details on the phase estimation of the full model). The bottom row shows the $O(\varepsilon)$ (blue) and $O(\varepsilon^2)$ (black) phase models exhibiting qualitatively similar phase dynamics at $\varepsilon=0.005$ (E) and $\varepsilon=0.016$ (G), respectively. Corresponding time traces are shown to the right of each portrait, e.g., panel (B) corresponds to (A), and (F) corresponds to (E).

Parameter	Value
\overline{C}	$1 \mu \mathrm{F/cm}^2$
E_k	-90 mV
E_{Na}	50 mV
$E_{ m t}$	$0~\mathrm{mV}$
$E_{ m L}$	-70 mV
$E_{\rm syn}$	0 mV (Figure 3) or -100 mV (Figure 5)
$g_{ m L}$	$0.05\mathrm{mS/cm^2}$
g_{K}	$5\mathrm{mS/cm}^2$
$g_{ m Na}$	$3\mathrm{mS/cm}^2$
$g_{\mathrm{syn}} \equiv \varepsilon$	$0\mathrm{mS/cm}^2$ to $0.027\mathrm{mS/cm}^2$
α	3
β	2
σ_T	0.8
$V_{ m T}$	20 mV
I_{app}	$0.8\mu A/cm^2$ (Figure 3) or $0.6\mu A/cm^2$ (Figure 5)

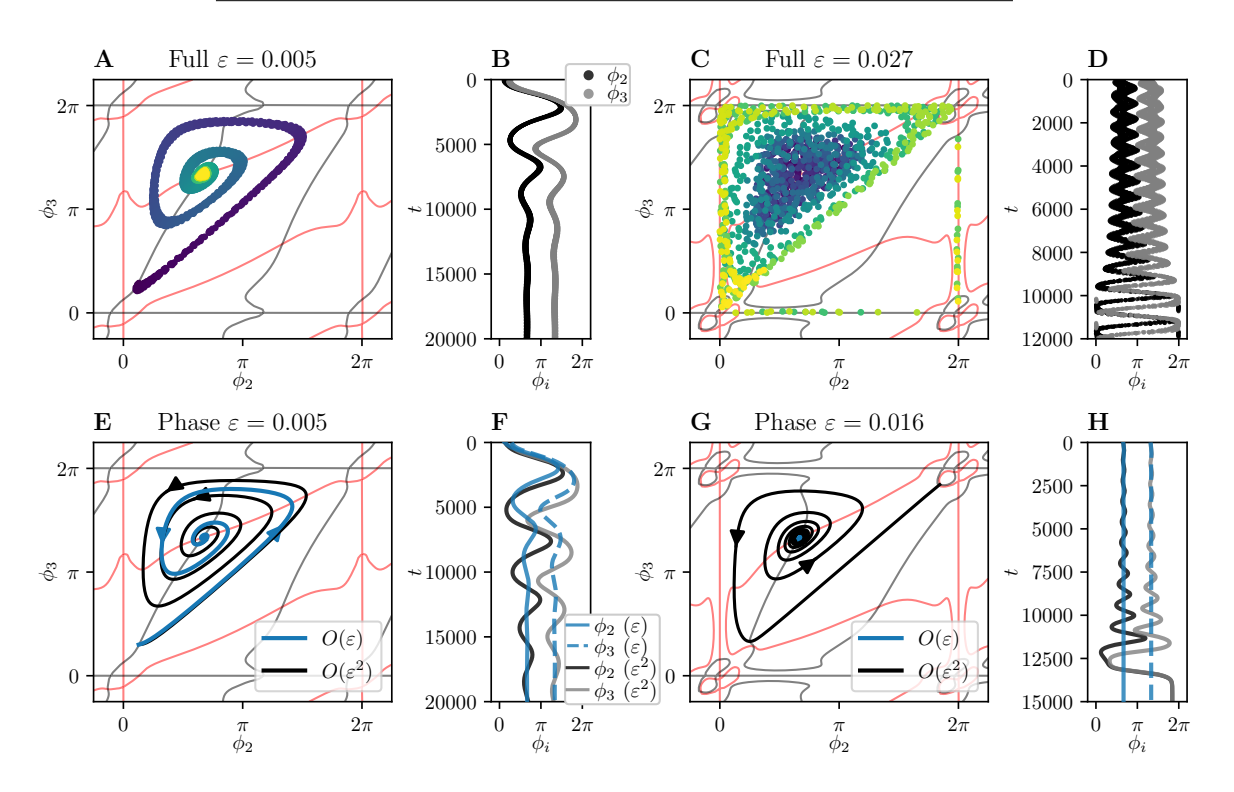


Figure 3. Comparison of the full (top row) and reduced (bottom row) thalamic models. All panels show the corresponding nullclines of the $O(\varepsilon^2)$ reduced model. (A) Phase difference estimate of the full model dynamics. Lighter shades indicate later times. (E) The reduced models $(O(\varepsilon))$ blue and $O(\varepsilon^2)$ black) at the approximate corresponding coupling strength. Note that the $O(\varepsilon)$ model remains at the splay state. Arrows indicate movement in forward time. (B), (F) Corresponding plots over time of the full model and reduced model, respectively. (C), (D), Full and reduced model dynamics, respectively. (D), (H) Corresponding plots over time of the full and reduced models, respectively. Parameters as in Table 1 with $E_{\rm syn}=0$ mV and $I_{\rm app}=0.8~\mu{\rm A/cm}^2$. We show every hundredth time point of the full model phase estimation.

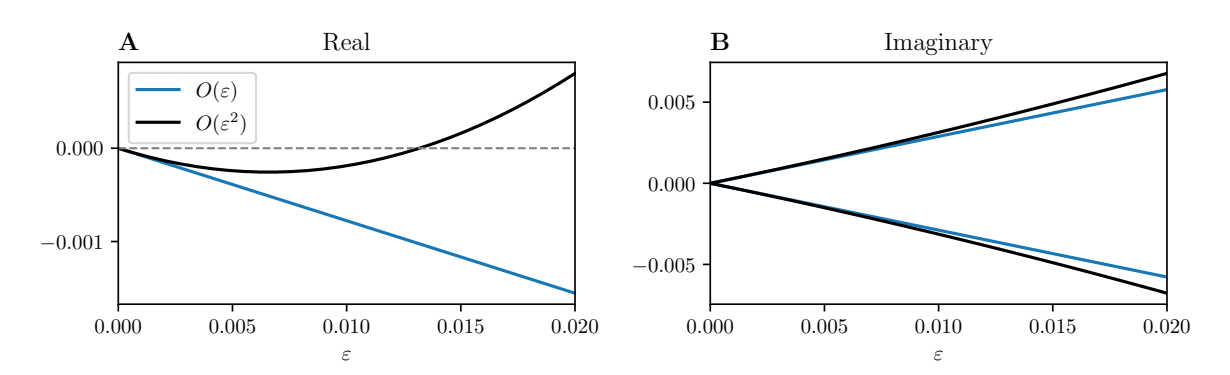


Figure 4. Real (A) and imaginary (B) parts of the eigenvalues of the Jacobian matrix evaluated at the splay state in the reduced thalamic models. Blue: $O(\varepsilon)$; orange: $O(\varepsilon^2)$; black: $O(\varepsilon^3)$. The dashed line is provided for reference to highlight the loss of stability as ε increases in higher-order accuracy models. Parameters are identical to those used in Figure 3.

At $\varepsilon = 0.005$, the full model phase differences tend towards an asymptotically stable splay state when initialized near synchrony with phases $(\phi_2, \phi_3) = (0.4, 1)$ ((A), (B), where $\phi_i \in [0, 2\pi)$). With the same initial values, all $O(\varepsilon)$ (blue) and $O(\varepsilon^2)$ (black) phase models coincide with the full model at, as expected, (panels (E), (F)).

For greater values of ε , phase differences in the full model asymptotically tend towards a limit cycle oscillation (panels (C), (D)) and the $O(\varepsilon^2)$ reduced model tends towards synchrony. While the asymptotic dynamics differ, we nevertheless capture the loss of stability in the splay state (we checked the order $O(\varepsilon^3)$ term, but found no improvement in the reduced solution). Real and imaginary parts of the Jacobian evaluated at the splay state are shown in Figure 4.

To further demonstrate the utility of our method, we show the phase reduction of the thalamic model for a different set of synaptic parameters: $E_{\rm syn}=0$ and $\varepsilon<0$. This choice is less biologically relevant because it corresponds to an excitatory chemical synapse with a negative conductance, but the goal of this example is to show that the reduced model can capture additional nonlinear dynamics in a model more complex than the CGL model.

Comparisons between the full and reduced versions of the thalamic model for this new parameter set are shown in Figure 5. The top row shows phase estimates of the full model for $\varepsilon = -0.008$ (A) and $\varepsilon = 0.0025$ (C), where lighter shades correspond to later times (see Appendix D for more details on the phase estimation of the full model). The bottom row shows the $O(\varepsilon)$ (blue) and $O(\varepsilon^2)$ (black) phase models exhibiting qualitatively similar phase dynamics at $\varepsilon = -0.0014$ (E) and $\varepsilon = 0.0025$ (G), respectively. Corresponding time traces are shown to the right of each portrait, e.g., panel (B) corresponds to (A), and (F) corresponds to (E).

The right column of Figure 5 (panels (C), (D) and (G), (H)) serves as a sanity check, where $\varepsilon > 0$ puts us back in a biologically realistic regime. The full and reduced models all tend towards synchrony; however, the $O(\varepsilon^2)$ model (black) captures the transient dynamics more accurately than the $O(\varepsilon)$ model.

At $\varepsilon = -0.008$, the full model phase differences exhibit a loss of stability in the splay state and the asymptotic dynamics tend towards a limit cycle (A), (B). The $O(\varepsilon^2)$ reduced model

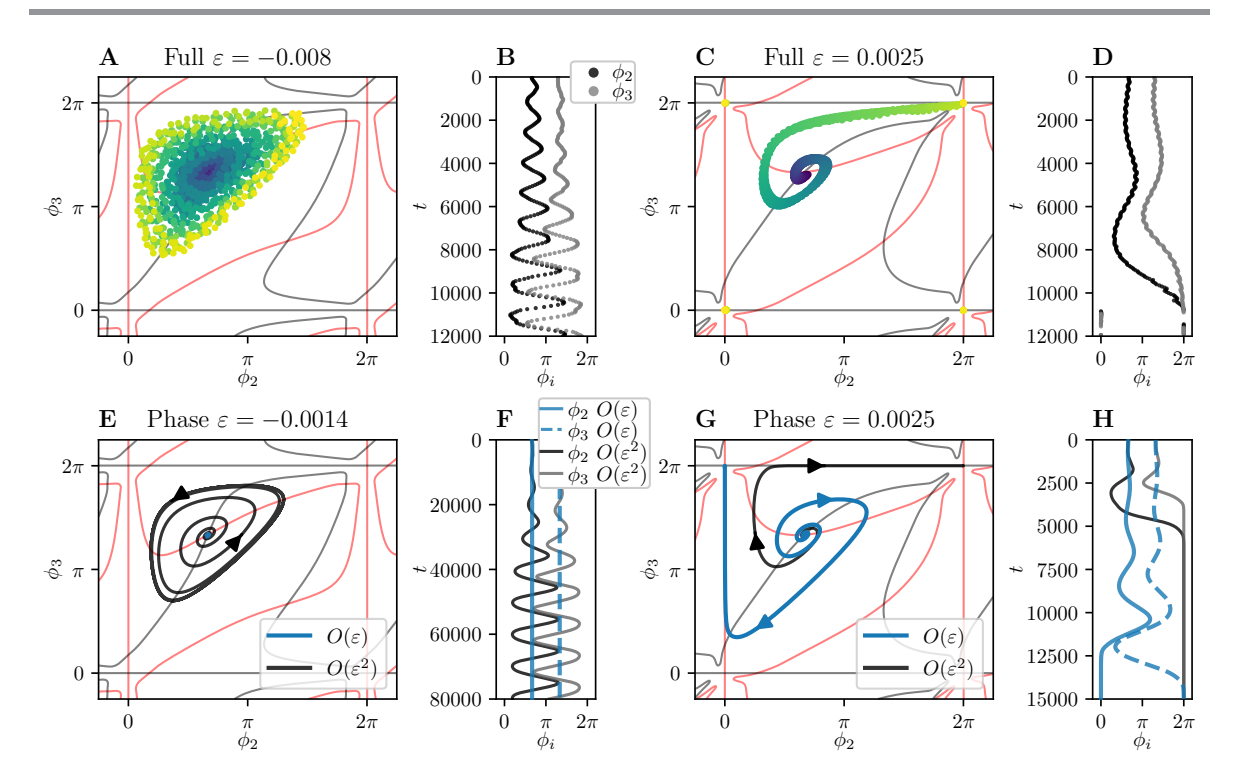


Figure 5. Comparison of the full (top row) and reduced (bottom row) thalamic models. All panels show the corresponding nullclines of the $O(\varepsilon^2)$ reduced model. (A) Phase difference estimate of the full model dynamics. Lighter shades indicate later times. (E) The reduced models $(O(\varepsilon))$ blue and $O(\varepsilon^2)$ black) at the approximate corresponding coupling strength. Note that the $O(\varepsilon)$ model remains at the splay state. Arrows indicate movement in forward time. (B), (F) Corresponding plots over time of the full model and reduced model, respectively. (C), (D) Full and reduced model dynamics, respectively. (D), (H) Corresponding plots over time of the full and reduced models, respectively. Parameters as in Table 1 with $E_{\rm syn} = -100\,{\rm mV}$ and $I_{\rm app} = 0.6\,{\rm \mu A/cm}^2$. We show every hundredth time point of the full model phase estimation.

captures this behavior ((E), (F), black), whereas the $O(\varepsilon)$ reduced model does not ((E), (F), blue). Note the considerable nonlinearity in the phase difference dynamics as a function of ε . Despite the small size of ε , the $O(\varepsilon)$ and $O(\varepsilon^2)$ dynamics differ substantially.

This example is affected by a nearby saddle-node on an invariant cycle (SNIC) bifurcation, which occurs just below the applied current value of $I_{\rm app}=0.6~\mu{\rm A/cm^2}$, and reminds us that "small" ε is relative. The first example of the thalamic model (Figure 3) uses much greater values of $\varepsilon=0.005$ and $\varepsilon=0.027$, the latter being an order of magnitude greater than in the current example (Figure 5). The proximity to a SNIC also highlights the shortcomings with our second assumption, where we use first-order averaging. The reciprocal of our period is $1/T=1/44~{\rm ms}\approx 0.023$, which places an approximate upper bound on the coupling strength ε , which must be much smaller than 1/T [32].

Nevertheless, we can compute changes in the stability of the splay state as in the previous examples. The real and imaginary parts of the eigenvalues of the Jacobian matrix evaluated at the splay state are shown in Figure 6. The $O(\varepsilon^2)$ model captures the loss in stability while the $O(\varepsilon)$ model does not.

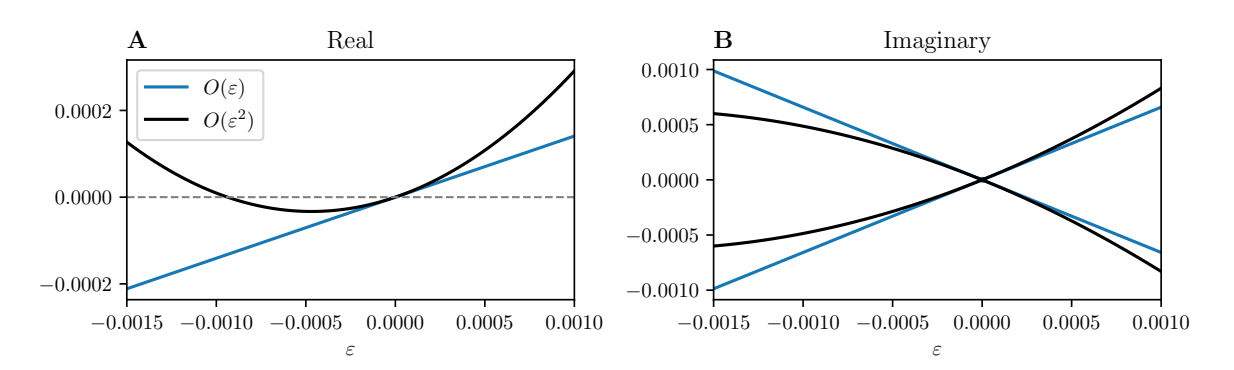


Figure 6. Real (A) and imaginary (B) parts of the eigenvalues of the Jacobian matrix evaluated at the splay state in the reduced thalamic models. Blue: $O(\varepsilon)$; orange: $O(\varepsilon^2)$; black: $O(\varepsilon^3)$. The dashed line is provided for reference to highlight the change of stability as ε increases in higher-order accuracy models. Parameters are identical to those used in Figure 5.

6. Discussion. In summary, we derived coupling functions that capture higher-order Nbody interactions while allowing for nontrivial effects from slowly decaying Floquet modes. While we did not consider heterogeneity, the formulation allows for the vector fields to be entirely different, so long as there exists a parameter in each system that can bring the oscillators to the same period, or alternatively, so long as the oscillator periods are similar in the absence of coupling. We applied our method to two systems, the CGL model and a thalamic neuron model. We found that higher-order terms were necessary to reproduce the dynamics of the original system. In the CGL model, even though the $O(\varepsilon^2)$ reduced model contained three-body interactions, it was the $O(\varepsilon^3)$ reduced model that captured additional nonlinearities, suggesting that in general, N-body interactions alone are not always sufficient to reproduce full model dynamics. In the thalamic model, we considered two examples, the first at $I_{\rm app}=0.8~\mu{\rm A/cm^2}~E_{\rm syn}=-100$ and the second at $I_{\rm app}=0.6~\mu{\rm A/cm^2}~E_{\rm syn}=0$. In the first example, we captured the loss in stability of the splay state using the $O(\varepsilon^2)$ model. In the second example, we explored beyond a biologically relevant parameter regime and observed limit cycle behavior in the phase difference of the full model for $g_{\text{syn}} \equiv \varepsilon < 0$, which the $O(\varepsilon^2)$ reduced model captured. We noted that the ε values between the full and reduced models differed more than in previous examples in capturing similar behaviors. This difference is likely due to the existence of a SNIC bifurcation just below the parameter value $I_{\rm app} = 0.6 \,\mu\text{A/cm}^2$.

Our method is both a generalization of existing methods that consider higher-order phase-isostable interactions and a general framework from which to study higher-order effects. For example, a higher-order reduced model is derived using the Haken-Kelso-Bunz (HKB) equation in [36]. The higher-order terms are the lowest-order Fourier terms of our \mathcal{H} functions; thus the same questions of existence can be answered with our method and further explored with additional Fourier terms and multibody interactions. Larger networks of the HKB equation that consider interactions well beyond dyadic [74] fit comfortably within the limitations of our method (see section 6.1 for details). Similarly, there is no restriction to applying our method to questions of coordinated movement, e.g., [25], or studies of coupled population dynamics [39].

Our method may aid in addressing questions of synchrony and phase-locking in general finite populations of coupled oscillators with heterogeneity where order parameters are

typically used. For example, the heterogeneous systems and coupling functions considered in [1] cannot exhibit synchrony and a "bounded synchronization" measurement [22] is necessary. Our method could provide a far more detailed understanding of the bounded synchronization state alongside other possible phase-locked states. Moreover, similar questions could be asked in much more realistic and complex neurobiological models.

Two recent results are most relevant to our work. The first is [34], where a phase-isostable description of coupled oscillators is derived for heterogeneous, planar oscillators. The authors' assumptions and handling of the isostable coordinate(s) are similar to ours (including earlier work [50]). In particular, their heterogeneous assumption is equivalent to ours in the following sense. If we let $\mu = 1, ..., M$ be the oscillator index for M oscillators, then we can directly transform our framework into theirs by taking $\delta_{\mu} \mathcal{Z}_{\mu}(\theta_{\mu}, \psi_{\mu}) \cdot Q_{i}(\theta_{\mu}, \psi_{\mu})$ to lowest order in ε , which is some constant $\delta_{\mu} \hat{d}$, say, and setting $1 + \delta_{\mu} \hat{d} = \omega_{\mu}$. Then our framework can be used to explore phase-locking and phase drift as a function of coupling strength and forcing frequency in the same manner. A key difference is that our framework allows oscillators of arbitrarily high dimension (not to mention that we publicly share our numerical methods under an open-source license [45]).

Finally, the remarkable work by Nicks, Allen, and Coombes [42] warrants special attention. They use both phase and isostable coordinates to derive conditions for the existence and stability of phase-locked states in networks of coupled oscillators. The isostable dynamics are kept explicit, which confers some advantages that our method may not. Indeed, the choice of "eliminating" the isostable dynamics in our work inevitably reduces the accuracy of our approximation, because we ignore potentially important transient effects. Moreover, analytical calculations become rapidly cumbersome for lower-order terms for even very simple models such that numerics become necessary beyond order 3 or 4. Their work highlights the importance of choosing methods with compatible assumptions when applying phase-isostable methods to one's own models. It may very well be worth increasing the accuracy of a reduced system in exchange for an increase in dimension. On the other hand, our method is useful if only pure phases are desired, while including at least some of the corrective effects of isostable dynamics.

6.1. Limitations. We begin with limits related to our implementation. If the \mathcal{H} functions have sparse Fourier modes, then a Fourier truncation can be used to greatly reduce the time complexity and memory requirements of our method (see Appendix A.1). In particular, knowledge of the exact types of functions that appear for each order is a significant part of this computational efficiency. However, the current implementation has only up to order $O(\varepsilon^3)$ implemented for the Fourier method. While it is clear that there is a pattern in the types of separable and nonseparable functions that appear in the Fourier terms as a function of higher orders, we have not precisely determined a formula for this pattern at the time of this writing. Once the pattern is fully understood, it will be possible to determine significantly higher-order interaction terms using the Fourier truncation.

Limitations related to the reduction method outside of our implementation center around the two key assumptions that make the derivation of this method possible. First, we assume that the timescale of phase $\theta_i - t$ (i.e., the phase equation after subtracting the moving frame) differs sufficiently from the timescale of the functions $p_i^{(k)}$ (the expansion terms of the isostable

coordinate ψ_i), such that θ_i terms can be taken out of a time integral. This assumption is reasonable for at least moderate values of ε up to $\varepsilon = 0.06$ in our examples, where the phase difference variables ϕ_i tend to vary relatively slowly. However, additional work must be done to more carefully examine this assumption for use in greater stronger coupling strengths ε .

Second, we use first-order averaging, which is technically valid for small ε comparable to those used in weak coupling theory. This limitation is especially apparent in the last example, where the thalamic model is near a SNIC bifurcation and the reciprocal of the period (1/44 ms \approx 0.023) places an approximate upper bound on the coupling strength ε , as ε must be much smaller than 1/T [32]. This example may benefit from higher-order averaging methods [31, 32]. In addition, we have observed phase drift in the full model (data not shown) in a manner that may not be possible to capture in the current formulation. For example, with N=3 homogeneous oscillators and some values of ε , two oscillators synchronize and the third exhibits a phase drift, effectively resulting in a two-oscillator system with a drift in the remaining phase difference. In our formulation, a single phase difference equation cannot exhibit drift without heterogeneity. This discrepancy may be due to ignoring transients in the isostable coordinates—if we were to include explicit isostable dynamics such as in [42], this behavior might be captured.

Appendix A. Numerical details for computing higher-order interaction functions. We briefly discuss three numerical methods for calculating \mathcal{H} functions.

A.1. Option 1: Averaging in terms of Fourier coefficients. If the expansion terms $g_i^{(k)}$, $\mathcal{Z}_i^{(k)}$, and $\mathcal{I}_i^{(k)}$ have sparse Fourier modes, it may be advantageous to calculate the \mathcal{H} functions in terms of Fourier coefficients. Given order k, define $\mathbf{\Theta} = (\theta_1, \dots, \theta_N)$ and $\mathbf{1} = (1, \dots, 1)$. Suppose that we wish to obtain an $\mathcal{H}_i^{(k)}$ function, so we apply first-order averaging to some order k function $f^{(k)}$ for a given system of N oscillators:

$$\int_0^T \bar{f}^{(k)}(\theta_1 + t, \dots, \theta_N + t) \, \mathrm{d}t.$$

The integrand $f^{(k)}$ is simply a placeholder for any of the terms that appear in the integrand in the calculation of \mathcal{H} functions, e.g., for k = 1, $f^{(1)}$ could be any integrand term here:

$$\sum_{j_1,j_2} \mathcal{H}_{ij_1j_2}(\xi_1,\xi_2) = \sum_{j_1,j_2} \frac{a_{ij_2}}{T} \int_0^T Z_i^{(0)}(s) \cdot v_{ij_1}^{(1,0)}(s,\xi+s) g_{ij_2}(s,\xi+s) \, \mathrm{d}s
+ \sum_{j_1,j_2} \frac{a_{j_1j_2}}{T} \int_0^T Z_i^{(0)}(s) \cdot v_{ij_1}^{(1,0)}(s,\xi_1+s) g_{j_1j_2}(\xi_1+s,\xi_2+s) \, \mathrm{d}s
+ \sum_{j_1,j_2} \frac{a_{ij_2}}{T} \int_0^T Z_i^{(0)}(s) \cdot K_{ij_1}^{(0)}(s,\xi_1+s) g_{ij_2}(s,\xi_2+s) \, \mathrm{d}s.$$

Consider the N-dimensional Fourier expansion of the integrand:

$$\int_0^T \sum_{\boldsymbol{m} \in \mathbb{Z}^N} c_{j,k,\boldsymbol{m}} e^{i\boldsymbol{m} \cdot (\boldsymbol{\Theta} + \mathbf{1}t)} \, \mathrm{d}t,$$

where $c_{j,k,m}$ are the Fourier coefficients given oscillator j and order k, and $m = (m_1, m_2, ..., m_N)$. We simplify this integral using straightforward integral properties and orthogonality of the Fourier basis:

(A.1)
$$\int_{0}^{T} \sum_{\boldsymbol{m} \in \mathbb{Z}^{N}} c_{i,k,\boldsymbol{m}} e^{i\boldsymbol{m} \cdot (\boldsymbol{\Theta} + 1t)} dt = \sum_{\boldsymbol{m} \in \mathbb{Z}^{N}} \int_{0}^{T} c_{i,k,\boldsymbol{m}} e^{i\boldsymbol{m} \cdot (\boldsymbol{\Theta} + 1t)} dt$$
$$= \sum_{\boldsymbol{m} \in \mathbb{Z}^{N}} c_{i,k,\boldsymbol{m}} e^{i\boldsymbol{m} \cdot \boldsymbol{\Theta}} \int_{0}^{T} e^{i\boldsymbol{m} \cdot 1t} dt$$
$$= \sum_{\boldsymbol{m} \cdot 1 = 0} c_{i,k,\boldsymbol{m}} e^{i\boldsymbol{m} \cdot \boldsymbol{\Theta}}.$$

That is, the only integral terms that remain are those such that the index vector m is orthogonal to the vector 1, and the integral of those surviving terms trivially evaluates to the scalar 1 (this calculation is a special case of [14]). Thus, the question of computing the average in time is simply a matter of computing the set of Fourier coefficients and extracting the relevant subset. If the number of oscillators N and mesh size K are large, then the desired averaged function in its final form can be taken as above; otherwise the desired functions can be found by the inverse Fourier transform.

Claim: The right-hand side of (A.1) depends on N-1 variables. Without loss of generality, suppose j=1. Now consider the change of variables $s=\theta_1+t$ and recall that $\phi_i=\theta_i-\theta_1$. Then rewriting (A.1) yields

$$\sum_{\boldsymbol{m}\in\mathbb{Z}^N} c_{1,k,\boldsymbol{m}} \int_0^T e^{i\boldsymbol{m}\cdot(s,\phi_2+s,\dots,\phi_N+s)} \,\mathrm{d}s = \sum_{\boldsymbol{m}\in\mathbb{Z}^N} c_{1,k,\boldsymbol{m}} \int_0^T e^{i[m_1s+m_2(\phi_2+s)+\dots+m_N(\phi_N+s)]} \,\mathrm{d}s$$

$$= \sum_{\boldsymbol{m}\in\mathbb{Z}^N} c_{1,k,\boldsymbol{m}} e^{i(m_2\phi_2+\dots+m_N\phi_N)} \int_0^T e^{is\boldsymbol{m}\cdot\mathbf{1}} \,\mathrm{d}s$$

$$= \sum_{\boldsymbol{m}\cdot\mathbf{1}=0} c_{1,k,\boldsymbol{m}} e^{i(m_2\phi_2+\dots+m_N\phi_N)},$$

where the last lines uses the orthogonality of the Fourier basis to evaluate the integral. Thus, we may easily evaluate (A.1) for N-1 phase differences by evaluating any one coordinate at zero.

While (A.1) is computationally efficient, we once again find that evaluating the underlying N-dimensional function to compute the Fourier coefficients of (A.1) requires significant amounts of memory. For example, evaluating an N-dimensional function on a mesh size of K again requires N^K points prior to taking the Fourier coefficient. So we seek an additional reduction in memory.

A.2. Option 2: Using an ODE solver as an adaptive mesh. In cases where the response functions (\mathcal{Z} and \mathcal{I}) and Floquet eigenfunctions have derivatives that greatly exceed their magnitudes, it is not possible to use only a small number of Fourier coefficients. Indeed, the thalamic model has a relatively large number of nontrivial Fourier modes for each order. For a uniform mesh, the number of points in the time-average integral grid K exceeds 1×10^7 , which is difficult to compute efficiently. Parallelizing this problem is further hindered by memory constraints.

Because the sharp peaks in the response functions and eigenfunctions tend to be in small regions of phase space, an adaptive mesh greatly reduces the number of integration points K. The most straightforward method is to use an ODE solver by rephrasing the time-average integration as an initial value problem. Given k, and $\theta_1, \ldots, \theta_N$, rewrite

$$\mathcal{H} = \frac{1}{T} \int_0^T \bar{h}_j^{(k)}(\theta_1 + t, \dots, \theta_N + t) dt$$

as

$$T\frac{d}{dt}\mathcal{H}(t) = \bar{h}_j^{(k)}(\theta_1 + t, \dots, \theta_N + t), \quad \mathcal{H}(0) = 0.$$

Then the desired time-average is given by $\mathcal{H}(T)$. If needed, the mesh is provided by the ODE solver. We use the Python [63] implementation of LSODA.

A.3. Option 3: Brute force and parallelization. If all else fails, it is possible to brute force calculations of the \mathcal{H} functions, especially if the network has $N \leq 3$ oscillators with only a few lower-order terms and a coarse mesh. Our Python implementation will attempt to use CPU parallelization, and if available, CUDA parallelization. Because the memory requirements grow exponentially as a function of mesh size, mesh sizes are typically restricted to 500 points for roughly 16GB of RAM. Running the code on a cluster with more CPUs is recommended (instructions are included in the repository with sample scripts).

Appendix B. Thalamic model. The remaining equations for the thalamic model are

$$I_{\rm L}(V) = g_{\rm L}(V-E_L), \quad I_{\rm Na} = g_{\rm Na}hm_{\infty}^3(V)(V-E_{\rm Na}),$$

 $I_{\rm K} = 0.75g_{\rm K}(1-h)^4(V-E_{\rm K}), \quad I_{\rm T} = g_{\rm T}rp_{\infty}^2(V)(V-E_{\rm T}),$

and

$$\begin{aligned} a_h(V) &= 0.128 \exp(-(V+46)/18), & b_h(V) &= 4/(1+\exp(-(V+23)/5)), \\ m_\infty(V) &= 1/(1+\exp(-(V+37)/7)), & h_\infty(V) &= 1/(1+\exp((V+41)/4)), \\ r_\infty(V) &= 1/(1+\exp((V+84)/4)), & p_\infty(V) &= 1/(1+\exp(-(V+60)/6.2)), \\ \tau_h(V) &= 1/(a_h(V)+b_h(V)), & \tau_r(V) &= 28+\exp(-(V+25)/10.5). \end{aligned}$$

Appendix C. Coupling function expansions. Recall our original coupled system (3.1),

$$\dot{X}_i = F_i(X_i) + \delta_i Q_i(X_i) + \varepsilon \left[\sum_{j=1}^N a_{ij} G_{ij}(X_i, X_j) \right], \quad i = 1, 2, \dots, N.$$

Here we provide a high-level description of the ε -expansion of the coupling functions G_{ij} . First, fix i and j and consider an arbitrary mth coordinate G_m of G_{ij} . Recall that we expand this function in the following manner:

(C.1)
$$G_m(\Lambda + \Delta \Xi) = G_m^{(0)}(\Lambda) + G_m^{(1)}(\Lambda) \Delta \Xi + \sum_{k=2}^{\infty} \frac{1}{k!} \left[\bigotimes^k \Delta \Xi^{\top} \right] \operatorname{vec} \left(G_m^{(k)}(\Lambda) \right),$$

where $\Delta\Xi = [\Delta x^{\top}, \Delta y^{\top}]^{\top} \in \mathbb{R}^{n_i + n_j}$, Λ is purely a function of θ_i and θ_j , and $\Delta x \approx \psi_i g_i^{(1)}(\theta_i) + \psi_i^2 g_i^{(2)}(\theta_i) + \cdots$, with Δy defined similarly. Writing $\Delta x = [\Delta x_1, \dots, \Delta x_{n_i}]^T$, each Δx_{ℓ} is a polynomial in ψ_i by definition (likewise for Δy_{ℓ}). It follows that $\overset{1}{\otimes} \Delta\Xi^{\top} \equiv \Delta\Xi$ only contains polynomials in ψ_i in the first n_i elements and polynomials in ψ_j in the last n_j elements. Thus, the term $G_m^{(1)}(\Lambda)\Delta\Xi$, which is equivalent to a dot product, is a scalar that consists of the sum of a polynomial in ψ_i with a sum of a polynomial in ψ_j . The next term in the expansion includes the cross-multiplication of the two polynomials:

where the square brackets only help organize the terms. This vector has the shape $1 \times (n_i + n_j)^2$ and contains polynomials of the form

$$(\psi_i c_1 + \psi_i^2 c_2 + \cdots)^{\ell} (\psi_j d_1 + \psi_j^2 d_2 + \cdots)^{(2-\ell)}$$

for some arbitrary scalars c_k , d_k , $k \in \mathbb{N}^+$, and for $0 \le \ell \le 2$. Thus, the scalar term

$$\begin{bmatrix} \stackrel{2}{\otimes} \Delta \Xi^\top \end{bmatrix} \operatorname{vec} \left(G_m^{(2)}(\Lambda) \right)$$

contains a sum of polynomials in ψ_i and ψ_j with minimum order 2. Indeed, continuing this argument for arbitrary k yields polynomials in ψ_i and ψ_j of minimum degree k in the scalar term

$$\begin{bmatrix} {}^k_{} \otimes \Delta \Xi^\top \end{bmatrix} \operatorname{vec} \left(G_m^{(k)}(\Lambda) \right).$$

Since m was chosen arbitrarily, it follows that each coordinate of G_{ij} contains the same types of polynomials, and we can express each term in (C.1) as polynomials with vector coefficients. We assume that the polynomial terms have been collected and let $v_{ij}^{(\ell_1,\ell_2)}(\theta_i,\theta_j)$ be the vector coefficient of the term $\psi_i^{\ell_1}\psi_j^{\ell_2}$. Then we may express the expansion of G_{ij} in terms of ψ_i and ψ_i :

$$G_{ij}(\Lambda(\theta_i, \theta_j) + \Delta\Xi(\theta_i, \theta_j, \psi_i, \psi_j)) = \sum_{k=0}^{\infty} \sum_{\ell=0}^{k} \psi_i^{\ell} \psi_j^{(k-\ell)} v_{i,j}^{(\ell,k-\ell)}(\theta_i, \theta_j).$$

Finally, we make the substitution $\psi_i = \varepsilon p_i^{(1)} + \varepsilon^2 p_i^{(2)} + \cdots$, yielding the following terms ordered in powers of ε :

$$\begin{split} O(\varepsilon^0) &: v_{ij}^{(0,0)}, \\ O(\varepsilon^1) &: p_i^{(1)} v_{ij}^{(1,0)} + p_j^{(1)} v_{ij}^{(0,1)}, \\ O(\varepsilon^2) &: p_i^{(2)} v_{ij}^{(2,0)} + p_j^{(2)} v_{ij}^{(0,2)} + (p_i^{(1)})^2 v_{ij}^{(2,0)} + (p_j^{(1)})^2 v_{ij}^{(0,2)} + p_i^{(1)} p_j^{(1)} v_{ij}^{(1,1)}, \\ O(\varepsilon^3) &: p_i^{(3)} v_{ij}^{(3,0)} + p_j^{(3)} v_{ij}^{(0,3)} + [p_i^{(1)} p_j^{(2)} + p_i^{(2)} p_j^{(1)}] v_{ij}^{(1,1)} + (p_i^{(1)})^3 v_{ij}^{(3,0)} + (p_j^{(1)})^3 v_{ij}^{(0,3)}, \\ &\vdots \end{split}$$

Thus, we have a more explicit form for the $K_{ij}^{(\ell)}$ ε -expansion terms of G_{ij} , assuming that $v_{ij}^{(\ell_1,\ell_2)}$ is known. The calculation of $v_{ij}^{(\ell_1,\ell_2)}$ is handled automatically by a symbolic package.

C.1. Thalamic model.

$$\begin{split} K_{ij}^{(0)} &= \frac{1}{C} [a_{ij} E_{\text{syn}} w_j - a_{ij} v_i w_j, 0, 0, 0]^\top, \\ K_{ij}^{(1)} &= \frac{1}{C} [a_{ij} E_{\text{syn}} g_{w_j}^{(1)} p_j^{(1)} - a_{ij} v_i g_{w_j}^{(1)} p_j^{(1)} - a_{ij} w_j g_{v_i}^{(1)} p_i^{(1)}, 0, 0, 0]^\top, \\ K_{ij}^{(2)} &= \frac{1}{C} \left[[l] \begin{array}{c} a_{ij} E_{\text{syn}} g_{w_j}^{(1)} p_j^{(2)} + a_{ij} E_{\text{syn}} g_{w_j}^{(2)} (p_j^{(1)})^2 - a_{ij} v_i g_{w_j}^{(1)} p_j^{(2)} - a_{ij} v_i g_{w_j}^{(2)} (p_j^{(1)})^2 \\ - a_{ij} w_j g_{v_i}^{(1)} p_i^{(2)} - a_{ij} w_j g_{v_i}^{(2)} (p_i^{(1)})^2 - a_{ij} g_{v_i}^{(1)} g_{w_j}^{(1)} p_j^{(1)} p_j^{(1)} \end{array}, 0, 0, 0 \right]^\top. \end{split}$$

Appendix D. Phase estimation. We briefly describe the phase estimation method used in the paper (which is very similar to the estimation done in [46]). Consider a model with state variables x_1, \ldots, x_n , and suppose that we have saved a T-periodic limit cycle trajectory (at $\varepsilon = 0$) to some array $[y_1, \ldots, y_n]$. Then for a given simulation, we can define the phase to be a point $\theta \in [0, T)$ that minimizes

$$dist(x_1(t) - y_1(\theta), \dots, x_n(t) - y_n(\theta)),$$

where

$$\operatorname{dist}(\Delta x_1, \dots, \Delta x_n) := \sqrt{(\Delta x_1)^2 + \dots + (\Delta x_n)^2}$$

By simulating nondimensionalized versions of the equations, we need not normalize by the variance as in [46]. This brute-force method is remarkably fast with appropriate vectorization.

Acknowledgment. The authors acknowledge Reviewer #2's diligence in checking many important details in this text. The reviewer's questions and suggestions significantly improved the paper's content and clarity.

REFERENCES

- [1] F. Alderisio, B. G. Bardy, and M. di Bernardo, Entrainment and synchronization in networks of Rayleigh-van der Pol oscillators with diffusive and Haken-Kelso-Bunz couplings, Biol. Cybernet., 110 (2016), pp. 151-169.
- [2] C. BICK, T. BÖHLE, AND C. KUEHN, Multi-population phase oscillator networks with higher-order interactions, Nonlinear Differential Equations Appl., 29 (2022), 64.
- [3] R. J. BUTERA, JR., J. RINZEL, AND J. C. SMITH, Models of respiratory rhythm generation in the pre-Bötzinger complex. II. Populations of coupled pacemaker neurons, J. Neurophysiol., 82 (1999), pp. 398-415.

- [4] C. C. CANAVIER AND S. ACHUTHAN, Pulse coupled oscillators and the phase resetting curve, Math. Biosci., 226 (2010), pp. 77–96, https://doi.org/10.1016/j.mbs.2010.05.001.
- [5] C. C. CANAVIER, F. G. KAZANCI, AND A. A. PRINZ, Phase resetting curves allow for simple and accurate prediction of robust N:1 phase locking for strongly coupled neural oscillators, Biophys. J., 97 (2009), pp. 59–73.
- [6] R. Chaudhuri, K. Knoblauch, M.-A. Gariel, H. Kennedy, and X.-J. Wang, A large-scale circuit mechanism for hierarchical dynamical processing in the primate cortex, Neuron, 88 (2015), pp. 419–431.
- [7] S. COOMBES, Neuronal networks with gap junctions: A study of piecewise linear planar neuron models, SIAM J. Appl. Dyn. Syst., 7 (2008), pp. 1101–1129, https://doi.org/10.1137/070707579.
- [8] S. COOMBES, Y. M. LAI, M. ŞAYLI, AND R. THUL, Networks of piecewise linear neural mass models, European J. Appl. Math., 29 (2018), pp. 869–890.
- [9] S. COOMBES, R. THUL, AND K. C. WEDGWOOD, Nonsmooth dynamics in spiking neuron models, Phys. D, 241 (2012), pp. 2042–2057.
- [10] M. CORAGGIO, P. DE LELLIS, AND M. DI BERNARDO, Convergence and synchronization in networks of piecewise-smooth systems via distributed discontinuous coupling, Automatica, 129 (2021), 109596.
- [11] J. Cui, C. C. Canavier, and R. J. Butera, Functional phase response curves: A method for understanding synchronization of adapting neurons, J. Neurophysiol., 102 (2009), pp. 387–398.
- [12] J. D. DA FONSECA AND C. V. ABUD, The Kuramoto model revisited, J. Stat. Mech. Theory Exp., 2018 (2018), 103204.
- [13] I. R. Epstein and J. A. Pojman, An Introduction to Nonlinear Chemical Dynamics: Oscillations, Waves, Patterns, and Chaos, Oxford University Press, 1998.
- [14] G. B. Ermentrout, n:m phase-locking of weakly coupled oscillators, J. Math. Biol., 12 (1981), pp. 327–342, https://doi.org/10.1007/BF00276920.
- [15] G. B. Ermentrout and N. Kopell, Frequency plateaus in a chain of weakly coupled oscillators, I., SIAM J. Math. Anal., 15 (1984), pp. 215–237, https://doi.org/10.1137/0515019.
- [16] G. B. ERMENTROUT, Y. PARK, AND D. WILSON, Recent advances in coupled oscillator theory, Philos. Trans. Roy. Soc. A, 377 (2019), 20190092, https://doi.org/10.1098/rsta.2019.0092.
- [17] G. B. Ermentrout and D. H. Terman, Mathematical Foundations of Neuroscience, Interdiscip. Appl. Math. 35, Springer, New York, 2010, https://doi.org/10.1007/978-0-387-87708-2.
- [18] E. GENGEL, E. TEICHMANN, M. ROSENBLUM, AND A. PIKOVSKY, High-order phase reduction for coupled oscillators, J. Phys. Complex., 2 (2021), 015005.
- [19] J. GOLOWASCH, F. BUCHHOLTZ, I. R. EPSTEIN, AND E. MARDER, Contribution of individual ionic currents to activity of a model stomatogastric ganglion neuron, J. Neurophysiol., 67 (1992), pp. 341–349.
- [20] M. GOLUBITSKY, L. M. MESSI, AND L. E. SPARDY, Symmetry types and phase-shift synchrony in networks, Phys. D, 320 (2016), pp. 9–18.
- [21] J. Guckenheimer, Isochrons and phaseless sets, J. Math. Biol., 1 (1975), pp. 259–273.
- [22] D. J. Hill and J. Zhao, Global synchronization of complex dynamical networks with non-identical nodes, in 2008 47th IEEE Conference on Decision and Control, IEEE, 2008, pp. 817–822.
- [23] I. Hunter, M. M. Norton, B. Chen, C. Simonetti, M. E. Moustaka, J. Touboul, and S. Fraden, Pattern formation in a four-ring reaction-diffusion network with heterogeneity, Phys. Rev. E, 105 (2022), 024310.
- [24] E. M. IZHIKEVICH, Dynamical Systems in Neuroscience: The Geometry of Excitability and Bursting, Comput. Neurosci., MIT Press, Cambridge, MA, 2007.
- [25] J. A. S. Kelso, Unifying large-and small-scale theories of coordination, Entropy, 23 (2021), 537.
- [26] N. KOPELL AND G. B. ERMENTROUT, Symmetry and phaselocking in chains of weakly coupled oscillators, Comm. Pure Appl. Math., 39 (1986), pp. 623–660.
- [27] Y. Kuramoto, *Chemical Oscillations, Waves, and Turbulence*, Springer Ser. Synergetics 19, Springer-Verlag, Berlin, 1984, https://doi.org/10.1007/978-3-642-69689-3.
- [28] M. D. KVALHEIM AND S. REVZEN, Existence and uniqueness of global Koopman eigenfunctions for stable fixed points and periodic orbits, Phys. D, 425 (2021), 132959.
- [29] I. LEÓN AND D. PAZÓ, Phase reduction beyond the first order: The case of the mean-field complex Ginzburg-Landau equation, Phys. Rev. E, 100 (2019), 012211.

- [30] I. LEÓN AND D. PAZÓ, Enlarged Kuramoto model: Secondary instability and transition to collective chaos, Phys. Rev. E, 105 (2022), L042201.
- [31] J. LLIBRE, D. D. NOVAES, AND M. A. TEIXEIRA, Higher order averaging theory for finding periodic solutions via Brouwer degree, Nonlinearity, 27 (2014), pp. 563–583, https://doi.org/10.1088/0951-7715/27/3/563.
- [32] M. MAGGIA, S. A. EISA, AND H. E. TAHA, On higher-order averaging of time-periodic systems: Reconciliation of two averaging techniques, Nonlinear Dynam., 99 (2020), pp. 813–836.
- [33] J. R. MAGNUS AND H. NEUDECKER, Matrix Differential Calculus with Applications in Statistics and Econometrics, John Wiley & Sons, 2019.
- [34] E. T. MAU, M. ROSENBLUM, AND A. PIKOVSKY, High-order phase reduction for coupled 2D oscillators, Chaos, 33 (2023), 101101.
- [35] A. MAUROY, I. MEZIĆ, AND J. MOEHLIS, Isostables, isochrons, and Koopman spectrum for the actionangle representation of stable fixed point dynamics, Phys. D, 261 (2013), pp. 19–30.
- [36] J. McKinley, M. Zhang, A. Wead, C. Williams, E. Tognoli, and C. Beetle, Third party stabilization of unstable coordination in systems of coupled oscillators, J. Phys. Conf. Ser., 2090 (2021), 012167.
- [37] A. MEURER, C. P. SMITH, M. PAPROCKI, O. ČERTÍK, S. B. KIRPICHEV, M. ROCKLIN, A. KUMAR, S. IVANOV, J. K. MOORE, S. SINGH, T. RATHNAYAKE, S. VIG, B. E. GRANGER, R. P. MULLER, F. BONAZZI, H. GUPTA, S. VATS, F. JOHANSSON, F. PEDREGOSA, M. J. CURRY, A. R. TERREL, Š. ROUČKA, A. SABOO, I. FERNANDO, S. KULAL, R. CIMRMAN, AND A. SCOPATZ, SymPy: Symbolic computing in Python, PeerJ Comput. Sci., 3 (2017), e103, https://doi.org/10.7717/peerj-cs.103.
- [38] I. MEZIĆ, Spectrum of the Koopman operator, spectral expansions in functional spaces, and state-space geometry, J. Nonlinear Sci., 30 (2020), pp. 2091–2145.
- [39] R. MILNE AND F. GUICHARD, Coupled phase-amplitude dynamics in heterogeneous metacommunities, J. Theoret. Biol., 523 (2021), 110676.
- [40] R. E. MIROLLO AND S. H. STROGATZ, Synchronization of pulse-coupled biological oscillators, SIAM J. Appl. Math., 50 (1990), pp. 1645–1662, https://doi.org/10.1137/0150098.
- [41] B. Monga, D. Wilson, T. Matchen, and J. Moehlis, *Phase reduction and phase-based optimal control for biological systems: A tutorial*, Biol. Cybernet., 113 (2019), pp. 11–46.
- [42] R. Nicks, R. Allen, and S. Coombes, Insights into oscillator network dynamics using a phase-isostable framework, Chaos, 34 (2024), 013141.
- [43] R. Nicks, L. Chambon, and S. Coombes, Clusters in nonsmooth oscillator networks, Phys. Rev. E, 97 (2018), 032213.
- [44] E. Ott and T. M. Antonsen, Low dimensional behavior of large systems of globally coupled oscillators, Chaos, 18 (2008), 037113.
- [45] Y. Park, youngmp/nbody: v0.3.0-alpha, Zenodo, 2024, https://doi.org/10.5281/zenodo.10934036.
- [46] Y. PARK AND G. B. ERMENTROUT, Weakly coupled oscillators in a slowly varying world, J. Comput. Neurosci., 40 (2016), pp. 269–281, https://doi.org/10.1007/s10827-016-0596-6.
- [47] Y. PARK AND G. B. ERMENTROUT, A multiple timescales approach to bridging spiking- and populationlevel dynamics, Chaos, 28 (2018), 083123.
- [48] Y. PARK, S. HEITMANN, AND G. B. ERMENTROUT, The utility of phase models in studying neural synchronization, in Computational Models of Brain and Behavior, A. A. Moustafa, ed., Wiley Online Library, 2017, pp. 493–504.
- [49] Y. Park, K. M. Shaw, H. J. Chiel, and P. J. Thomas, The infinitesimal phase response curves of oscillators in piecewise smooth dynamical systems, European J. Appl. Math., 29 (2018), pp. 905–940.
- [50] Y. Park and D. D. Wilson, High-order accuracy computation of coupling functions for strongly coupled oscillators, SIAM J. Appl. Dyn. Syst., 20 (2021), pp. 1464–1484, https://doi.org/10.1137/20M1371208.
- [51] A. PÉREZ-CERVERA, T. M. SEARA, AND G. HUGUET, Global phase-amplitude description of oscillatory dynamics via the parameterization method, Chaos, 30 (2020), 083117.
- [52] C. S. Peskin, Mathematical Aspects of Heart Physiology, Courant Institute Lecture Notes, Courant Institute of Mathematical Sciences, New York University, New York, 1975.

- [53] C. K. PFEFFER, M. XUE, M. HE, Z. J. HUANG, AND M. SCANZIANI, Inhibition of inhibition in visual cortex: The logic of connections between molecularly distinct interneurons, Nat. Neurosci., 16 (2013), pp. 1068-1076.
- [54] B. PIETRAS AND A. DAFFERTSHOFER, Network dynamics of coupled oscillators and phase reduction techniques, Phys. Rep., 819 (2019), pp. 1–105.
- [55] M. ROSENBLUM AND A. PIKOVSKY, Numerical phase reduction beyond the first order approximation, Chaos, 29 (2019), 011105.
- [56] J. E. Rubin and D. Terman, High frequency stimulation of the subthalamic nucleus eliminates pathological thalamic rhythmicity in a computational model, Comput. Neurosci., 16 (2004), pp. 211–235.
- [57] S. SHIRASAKA, W. KUREBAYASHI, AND H. NAKAO, Phase-amplitude reduction of transient dynamics far from attractors for limit-cycling systems, Chaos, 27 (2017), 023119.
- [58] P. S. SKARDAL AND A. ARENAS, Higher order interactions in complex networks of phase oscillators promote abrupt synchronization switching, Commun. Phys., 3 (2020), 218.
- [59] P. S. SKARDAL, E. Ott, and J. G. Restrepo, Cluster synchrony in systems of coupled phase oscillators with higher-order coupling, Phys. Rev. E, 84 (2011), 036208.
- [60] S. H. STROGATZ, D. M. ABRAMS, A. MCROBIE, B. ECKHARDT, AND E. OTT, Crowd synchrony on the millennium bridge, Nature, 438 (2005), pp. 43–44.
- [61] T. Tanaka and T. Aoyagi, Multistable attractors in a network of phase oscillators with three-body interactions, Phys. Rev. Lett., 106 (2011), 224101.
- [62] C. M. Thibeault and N. Srinivasa, Using a hybrid neuron in physiologically inspired models of the basal ganglia, Front. Comput. Neurosci., 7 (2013), 88.
- [63] G. VAN ROSSUM AND F. L. DRAKE, Python 3 Reference Manual, CreateSpace, Scotts Valley, CA, 2009.
- [64] S. VON DER GRACHT, E. NIJHOLT, AND B. RINK, A Parametrisation Method for High-Order Phase Reduction in Coupled Oscillator Networks, preprint, arXiv:2306.03320, 2023.
- [65] K. C. A. Wedgwood, K. K. Lin, R. Thul, and S. Coombes, *Phase-amplitude descriptions of neural oscillator models*, J. Math. Neurosci., 3 (2013), 2.
- [66] D. Wilson, Phase-amplitude reduction far beyond the weakly perturbed paradigm, Phys. Rev. E., 101 (2020), 022220.
- [67] D. WILSON AND G. ERMENTROUT, Greater accuracy and broadened applicability of phase reduction using isostable coordinates, J. Math. Biol., 76 (2018), pp. 37–66, https://doi.org/10.1007/s00285-017-1141-6.
- [68] D. WILSON AND B. ERMENTROUT, An operational definition of phase characterizes the transient response of perturbed limit cycle oscillators, SIAM J. Appl. Dyn. Syst., 17 (2018), pp. 2516–2543, https://doi.org/10.1137/17M1153261.
- [69] D. WILSON AND B. ERMENTROUT, Phase models beyond weak coupling, Phys. Rev. Lett., 123 (2019), 164101.
- [70] D. Wilson and J. Moehlis, Isostable reduction of periodic orbits, Phys. Rev. E, 94 (2016), 052213.
- [71] D. WILSON AND J. MOEHLIS, Recent advances in the analysis and control of large populations of neural oscillators, Annu. Rev. Control, 54 (2022), pp. 327–351.
- [72] A. T. Winfree, *The Geometry of Biological Time*, Interdiscip. Appl. Math. 12, Springer Science & Business Media, 2001.
- [73] Y. ZANG AND E. MARDER, Neuronal morphology enhances robustness to perturbations of channel densities, Proc. Natl. Acad. Sci. USA, 120 (2023), e2219049120, https://doi.org/10.1073/pnas.2219049120.
- [74] M. Zhang, C. Beetle, J. A. S. Kelso, and E. Tognoli, Connecting empirical phenomena and theoretical models of biological coordination across scales, J. R. Soc. Interface, 16 (2019), 20190360.